CHAPTER 2: SYNTHESIS AND CHARACTERIZATION OF Pt(POP-BF$_2$)$^{4-}$

As discussed in Chapter 1, Pt(pop)$^{4-}$ participates in and facilitates a wide array of reactions. In its excited state, [Pt(pop)$^{4-}$]* is able to abstract hydrogen atoms from a variety of substrates including stannanes, silanes, alcohols, and hydrocarbons. It also reacts readily with alkyl and aryl halides (R or RX) to form the axially substituted Pt^{III}-Pt^{III} oxidative addition product (i.e. [Pt(pop)-RX]$^{4-}$ or [Pt(pop)-X$_2$]$^{4-}$) and, in the case of dihalide, the corresponding organic radical coupling product R$_2$.

In the late 1980s, Harvey prepared a fluoroborated analog of Pt(pop)$^{4-}$ by reaction with gaseous BF$_3$; however, the method replaced on average only six of the protons with BF$_2$ groups rather than the full eight replacements needed to form a complete covalent cage of bridging BF$_2$ groups. Unsurprisingly, the mix of constitutional isomers produced (Figure 1) via partial fluoroboration made the compound troublesome to purify. Presumably, this also explains why

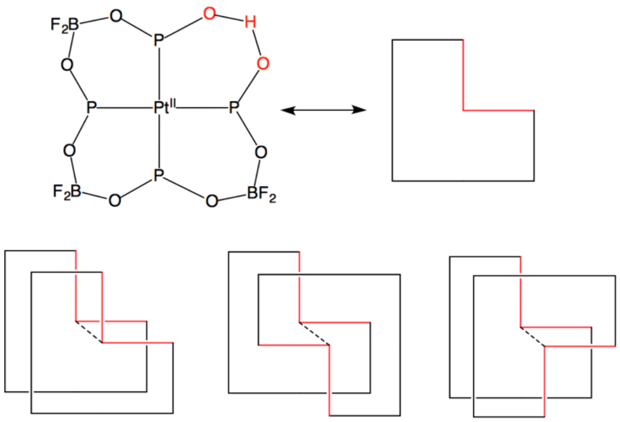

Figure 1: Schematic representation of the possible isomers resulting from the replacement of six of Pt(pop)'s eight protons with BF$_2$ groups, assuming neither half of the Pt$_2$ dimer experiences full replacement.[1]

Harvey was not able at the time to rigorously determine the compound's properties, particularly with respect to NMR signatures.[1]

In 2011, Yan-Choi Lam and collaborators in the lab of John Bercaw developed a more robust and reliable synthetic method for producing Pt(pop-BF$_2$)$^{4-}$ by stirring Pt(pop)$^{4-}$ in neat boron trifluoride diethyletherate (BF$_3$•Et$_2$O) for several days.[2] Initial experiments performed by Durrell, Lam, and Keller indicated that Pt(pop-BF$_2$)$^{4-}$, as predicted by Harvey, possessed unique luminescence properties that clearly differentiated it from its parent, Pt(pop)$^{4-}$.[2] In late 2012, intrigued by this relatively new and unexplored compound, I decided to devote my doctoral research to its study.

2.1 Synthetic developments

Before embarking on more complex analytical studies of Pt(pop-BF$_2$)$^{4-}$'s luminescence and reactivity, I first endeavored to corroborate the basic synthetic and luminescence results reported by Durrell and coworkers. As a result, I further developed Lam's synthesis of Pt(pop-BF$_2$)$^{4-}$ by improving the glassware setup and work-up techniques to decrease the possibility of exposure to BF$_3$•Et$_2$O or its hydration product, hydrofluoric acid (see section 2.4.6).

During this process, the tetraphenylphosphonium (Ph$_4$P$^+$) salt of Pt(pop-BF$_2$)$^{4-}$ was crystallized and characterized via X-ray diffraction for the first time (Figure 2). Prior to this point, only the tetrabutylammonium ((*n*-Bu)$_4$N$^+$) salt had been reported in the literature, although the tetraphenylarsonium (Ph$_4$As$^+$) salt had also been accessed by Lam.[2-4] In [Ph$_4$P]$_4$[Pt(pop-BF$_2$)], the distance between the largest electron density maxima is 2.85 Å, which corresponds to the Pt-Pt distance. However, the compound crystallizes in the monoclinic space group P2$_1$/*n* with only half

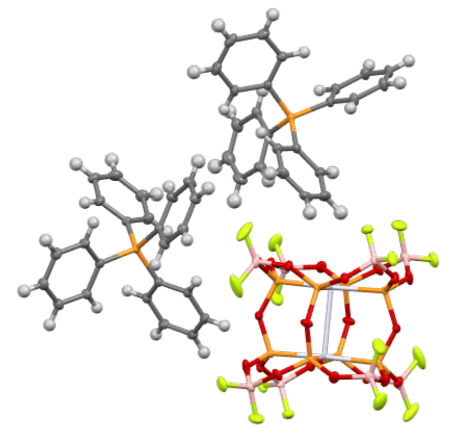

Figure 2: Crystal structure of $[Ph_4P]_4[Pt(pop\text{-}BF_2)]$.

of the molecule and two tetraphenylphosphonium cations in the asymmetric unit. Attempts to refine the density maxima as a second platinum position were unsuccessful; this could account for the slight discrepancy between this 2.85 Å distance and Lam's previously reported value of 2.89 Å for the tetraphenylarsonium salt of $Pt(pop\text{-}BF_2)^{4-}$.[4] Both the Pt-Pt distance values for salts of $Pt(pop\text{-}BF_2)^{4-}$ are significantly smaller than the value of 2.93 Å reported for $K_4Pt(pop)$; this could be attributed to the overall contraction of the Pt-Pt unit due to the rigidity of the BF_2 covalent "cage."[4,5] X-ray data are tabulated in Table 1 through Table 5 in section 2.6.

2.2 Basic luminescence properties

With the goal of duplicating the values for E_a, k_r and k_0 obtained by Durrell and coworkers, solutions of $Pt(pop\text{-}BF_2)^{4-}$ in acetonitrile were analyzed via both time-resolved and steady-state techniques to obtain values for fluorescence lifetime and quantum yield. With values for fluorescence lifetime and quantum yield in hand, values for $E_a, k_r,$ and k_0 can be calculated. These new data were compared directly to the values published in 2012.

2.2.1 Theoretical basis

In their 1992 publication probing the luminescence lifetimes of $Pt(pop)^{4-}$, Milder and Brunschwig presented an elegant series of experiments and equations for combining time-resolved and steady-state data taken at various temperatures to determine the activation energy of intersystem crossing between the singlet and triplet excited states, as well as the rates of radiative and nonradiative decay from the singlet state. These equations were applied to $Pt(pop-BF_2)^{4-}$ by Durrell and coworkers.

In $Pt(pop-BF_2)^{4-}$, analogously to $Pt(pop)^{4-}$, an electron in the singlet excited state has several pathways available by which to return to the ground state. It may nonradiatively decay (that is, decay without emitting a photon) or radiatively decay by emitting a photon (fluorescence). Nonradiative decay may occur either by intersystem crossing to the triplet state or by nonemissive decay to the ground state (for example, due to energy loss from solvent interactions). The rate of nonemissive decay to the ground state is represented by the rate constant k_d while the rate of intersystem crossing is represented by the rate constant k_{ISC}; the rate of radiative decay is denoted by k_r. Therefore, the total amount of nonradiative decay may be represented by the sum of k_d and k_{ISC}. As proposed by Milder and Brunschwig for $Pt(pop)^{4-}$, k_{ISC} for $Pt(pop-BF_2)^{4-}$ is presumed to follow Arrhenius-like behavior.

$$k_{nr} = k_d + k_{ISC} = k_d + \left(k_0 + \frac{A}{\sqrt{k_B T}} e^{-\frac{E_a}{k_B T}}\right) \qquad (1)$$

Meanwhile, the fluorescence lifetime (τ_{fl}) is inversely proportional to the rates of the decay paths out of the excited state:

$$\frac{1}{\tau_{fl}} = k_r + k_{nr} = k_r + k_d + k_0 + \frac{A}{\sqrt{k_B T}} e^{-\frac{E_a}{k_B T}} \qquad (2)$$

The lifetime τ_{fl} may be extracted from a luminescence-decay plot. By observing τ_{fl} at various temperatures, the following relation derived from equation (2) used with an appropriate fitting program may be used to find values for the unknowns A, E_a, and $k_r + k_d + k_0$.

$$y = \frac{1}{\tau_{fl}}$$

$$x = \frac{1}{T}$$

$$y = \alpha + \frac{\beta\sqrt{x}}{\sqrt{0.695}} e^{\frac{-\gamma x}{0.695}} \qquad (3)$$

in which

$$\alpha = k_r + k_d + k_0 \approx k_r + k_0$$

$$\beta = A$$

$$\gamma = E_a$$

Finally, the quantum yield (Φ) of a radiation-induced process is the number of times a specific event occurs per photon absorbed by the system. In this case, the quantum yield describes the ratio of photons emitted through fluorescence to total photons absorbed. Photons emitted through fluorescence can be equated to the radiative decay rate k_r, while total photon absorption is equal to the sum of the rates of all decay pathways: $k_r + k_{nr}$.

$$\Phi_{fl} = \frac{k_r}{k_r + k_{nr}} \qquad (4)$$

Equations (1) and (4) can be combined to give an expression for quantum yield that is dependent on k_r, k_d, k_0, E_a, and the temperature T.

$$\frac{1}{\Phi_{fl}} = \frac{k_{nr} + k_r}{k_r} = 1 + \frac{k_{nr}}{k_r} = 1 + \frac{k_d + k_0}{k_r} + \frac{A}{k_r\sqrt{k_B T}} e^{-\frac{E_a}{k_B T}} \qquad (5)$$

Φ_{fl} is difficult to directly observe, but in an optically dilute sample, the method of Williams, Winfield, and Miller may be used to calculate the quantum yield of un unknown Φ_x. In this method, the emission intensity of the unknown is compared to that of a reference possessing a known quantum yield Φ_r.[6-9] This comparison is based on Beer's law and is detailed in equation (6).

$$\Phi_x = \Phi_r \left(\frac{A_r(\lambda_r)}{A_x(\lambda_x)}\right)\left(\frac{I(\lambda_r)}{I(\lambda_x)}\right)\left(\frac{n_x^2}{n_r^2}\right)\left(\frac{D_x}{D_r}\right) \tag{6}$$

in which

$$\Phi_x = quantum\ yield\ of\ unknown$$
$$\Phi_r = quantum\ yield\ of\ reference\ compound\ (tabulated)$$
$$A(\lambda) = absorbance\ per\ cm\ of\ solution\ at\ excitation\ wavelength\ \lambda$$
$$I(\lambda) = relative\ intensity\ of\ excitation\ light\ at\ \lambda$$
$$n = average\ refractive\ index\ of\ solvent$$
$$D = integrated\ area\ under\ emission\ spectrum$$

With temperature-dependent quantum yield data in hand, the following function extracted from equation (5) used with an appropriate fitting program may be used to extract relations for $k_0, k_r, A,$ and E_a.

$$y = \frac{1}{\Phi_{fl}} \qquad x = \frac{1}{T} \qquad y = 1 + a + \frac{b\sqrt{x}}{\sqrt{0.695}} e^{\frac{-cx}{0.695}} \tag{7}$$

in which

$$a = \frac{k_d + k_0}{k_r} \approx \frac{k_0}{k_r}$$
$$b = \frac{A}{k_r}$$
$$c = E_a$$

The values calculated for the fitting parameters $a, b, c, \alpha, \beta,$ and γ using equations (3) and (7) can then be combined to obtain values for the unknowns $k_r, k_0, A,$ and E_a:

$$\begin{gathered} k_r = \frac{\beta}{b} \\ k_0 = \frac{\beta a}{b} \\ A = \beta \\ E_a = \gamma = c \end{gathered} \tag{8}$$

2.2.2 *Comparison to Durrell results*

Fluorescence lifetime and quantum yield data were acquired at temperatures ranging from 283 to 333 K.[i] Given that the quantum yield fitting program was written newly for this project (see Appendix 1) and relied on quantum yields derived from equation (6) using anthracene as the standard, the same fitting program used to fit our data was used to fit Durrell et al.'s raw data. These results were compared to Durrell's published results in order to assure the validity of our fitting program, and good agreement was found.[2] Results are summarized in Figure 3.

Fit parameter	**Value (2015 experiments)**	**Durrell value (with 2015 fitting program)**	**Durrell value (published, 2012)**
a	0.4269	0.5789	0.6 ± 0.1
b (cm$^{1/2}$)	2.547 x 10^6	1.73 x 10^6	1.73 x 10^6
c (cm^{-1})	2347	2232	2233 ± 75
α (s^{-1})	1.214 x 10^8		(2.55 ± 0.007) x 10^8
β (cm$^{1/2}$)	1.5 x 10^{14}		(3.0 ± 0.2) x 10^{14}
γ (cm^{-1})	2018		2229 ± 20

Figure 3: Temperature-dependent fluorescence lifetime and quantum yield fitting

With confidence in the validity of our fitting programs, we obtained several full sets of steady-state and time-resolved data. Values for a, b, and c were obtained using the absorbance and steady-state luminescence data presented in Figure 4; values for α, β, and γ were obtained using the time-resolved luminescence data presented in Figure 5. Our values are plotted against those obtained by Durrell et al. in Figure 6.

---

[i] Lifetime data were acquired with the kind assistance of Kana Takematsu.

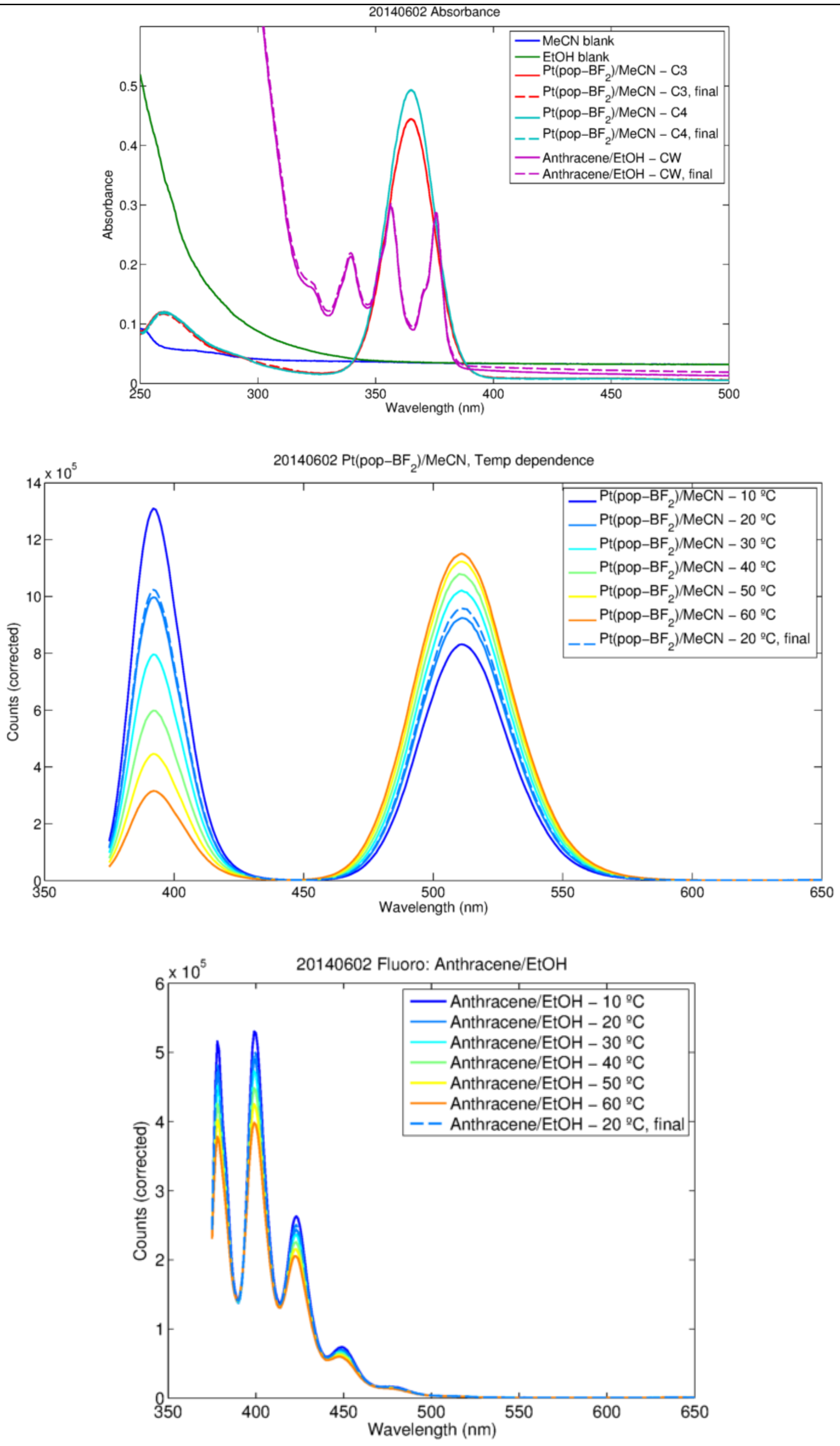

Figure 4: Absorbance data for $Pt(pop\text{-}BF_2)^{4-}$ and anthracene quantum yield standard (top) with steady-state luminescence data for $Pt(pop\text{-}BF_2)^{4-}$ (middle) and anthracene (bottom).

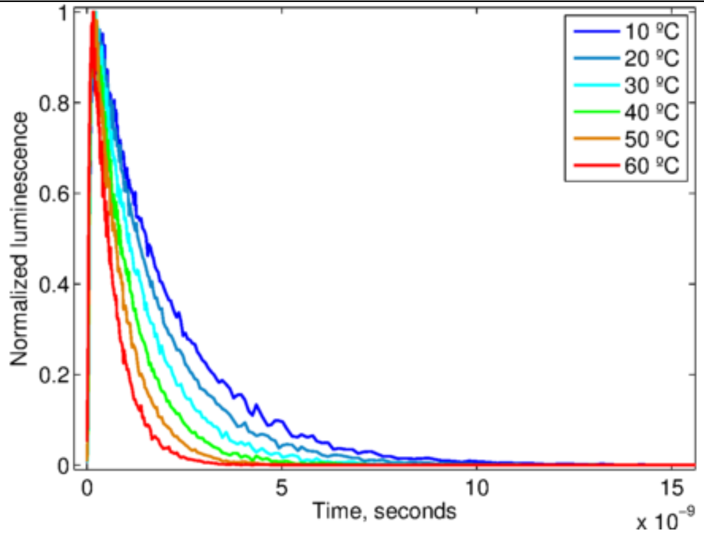

Figure 5: Temperature-dependent fluorescence lifetime data for Pt(pop-BF_2)$^{4-}$.

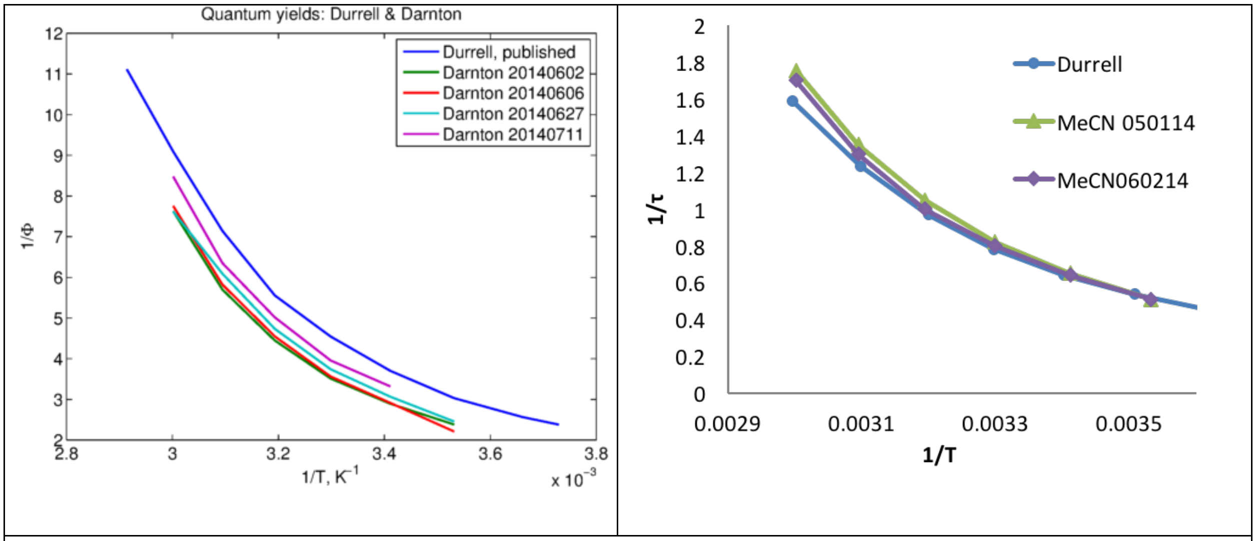

Figure 6: Data acquired in 2015 by Darnton & Takematsu vs. Durrell et al.; quantum yields (left), fluorescence lifetimes (right).

Anthracene was chosen as a quantum yield standard due to its well-documented behavior as well as the fact that it emits in the same region as Pt(pop-BF_2)$^{4-}$.[7,9-14] To ensure that equation (6) was being employed correctly, quinine sulfate was also employed as a standard to calculate both the quantum yield of Pt(pop-BF_2)$^{4-}$ and the quantum yield of anthracene itself; these data are presented in Figure 7 and summarized in Figure 8. Based on these results, it was concluded that anthracene was an appropriate standard for calculating the quantum yield of Pt(pop-BF$_2$)$^{4-}$ emission.

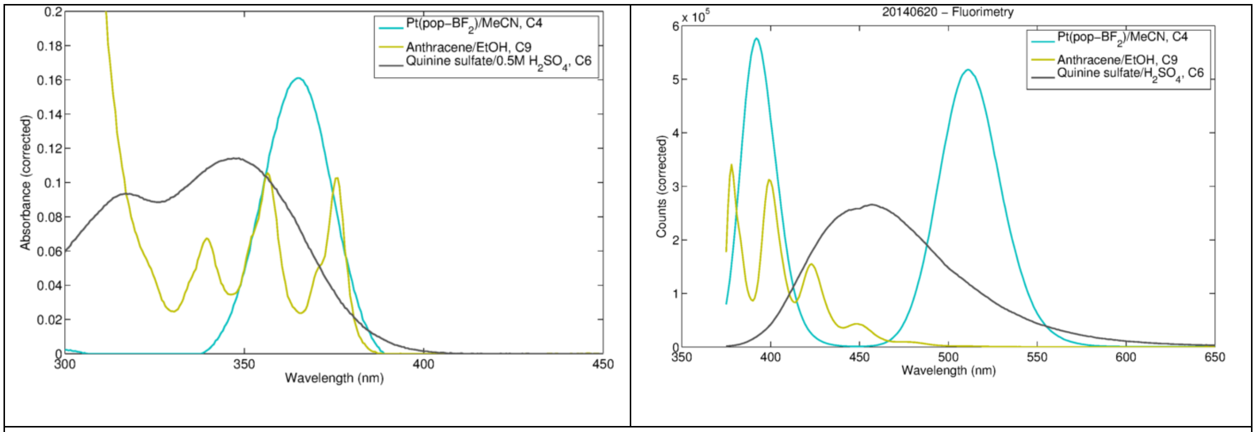

Figure 7: Pt(pop-BF$_2$)$^{4-}$, anthracene, and quinine sulfate absorbance (left) and luminescence (right) spectra.

Reference used	**Φ_{fl} (T=298 K)**	
	Pt(pop-BF$_2$)$^{4-}$	**Anthracene**
Anthracene	0.35	n/a
Quinine sulfate	0.31	0.22

Accepted values: Φ_{fl} Pt(pop-BF$_2$)$^{4-}$≈ 0.35; Φ_{fl} (anthracene) = 0.27[13]

Figure 8: Quantum yield tests

2.3 Pt(pop-BF$_2$)$^{4-}$ luminescence in different solvents

A study published in the early 1990s by Brunchschwig and Milder found that the rate of nonradiative decay for the singlet excited state in Pt(pop)$^{4-}$ had a strong dependency on solvent, particularly with regards to solvent polarity and the presence of exchangeable protons. After significant analysis, they concluded that the vibrations coupling the singlet and triplet state in

$Pt(pop)^{4-}$ are solvent modes and/or modes representing the interaction of the solvent with the $^1A_{2u}$ and $^3A_{2u}$ states of the complex along the Pt-Pt axial coordinate.[15]

It was expected that the rigidity and steric bulk of $Pt(pop\text{-}BF_2)^{4-}$, along with its lack of exchangeable ligands, would afford more protection from solvents. However, initial results reported by collaborator Tony Vlček indicated that Pt-Pt vibrational coherence in $Pt(pop\text{-}BF_2)^{4-}$ survived intersystem crossing and that the time constants were approximately equal to those found for $Pt(pop)^{4-}$. This raised the possibility that the Pt atoms in $Pt(pop\text{-}BF_2)^{4-}$ were not as well-shielded as we had previously thought them to be, and were perhaps still exposed to solvent molecules. With this in mind, experiments were undertaken to quantify the effect of solvent on $Pt(pop\text{-}BF_2)^{4-}$ excited state dynamics.

2.3.1 *Solvent choice and solvent stability*

Unfortunately, $Pt(pop\text{-}BF_2)^{4-}$ is much less soluble in common solvents than $Pt(pop)^{4-}$. All previous experiments involving $Pt(pop\text{-}BF_2)^{4-}$ were completed in acetonitrile, in which it is quite soluble. It is insoluble in less polar solvents like diethyl ether, toluene, and tetrahydrofuran, and decomposes in dichloromethane. While $Pt(pop\text{-}BF_2)^{4-}$ is soluble in dimethyl sulfoxide and dimethylformamide, such solvents are exceedingly difficult to keep anhydrous and uncontaminated due to their extreme polarity, in addition to being costly when purchased in the requisite high purities.

The greatest effects on the excited state dynamics of $Pt(pop)^{4-}$ were noted by Milder et al. in methanol and ethanol. As such, samples of ethanol and methanol were purified and dried according to published protocols.[16] $Pt(pop\text{-}BF_2)^{4-}$ proved to be insoluble in ethanol and only sparingly soluble in methanol, and it decomposed significantly in both methanol and methanol/acetonitrile mixtures as noted by significant broadening of the characteristic absorbance maximum at 365 nm. This was followed by a loss of absorption intensity and a slight blue-shift in wavelength over 24 hours (Figure 9).

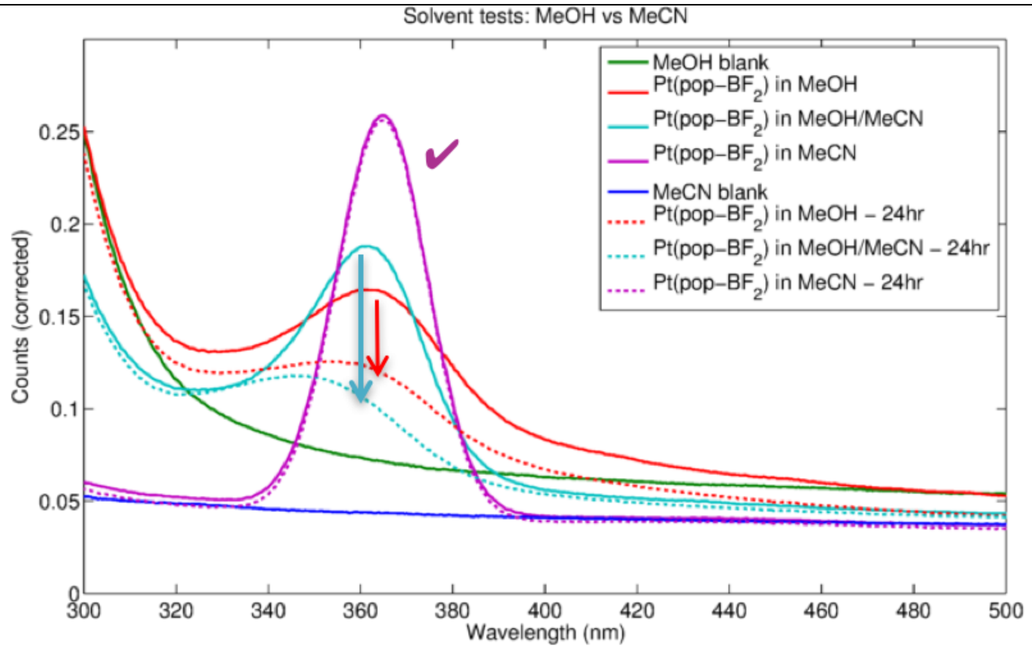

Figure 9: Stability of Pt(pop-BF$_2$)$^{4-}$ over 24 hours in acetonitrile, acetonitrile/methanol, and methanol. Absorbance profile is maintained in acetonitrile (purple); immediate peak broadening and loss of intensity over time noted in acetonitrile/methanol (blue) and methanol (red).

This decomposition in methanol is attributed, at least initially, to removal of the BF$_2$ groups by protonation to reform Pt(pop)$^{4-}$. This is supported by steady-state fluorescence data obtained in the same solvents; the emission maxima and the relative sizes of the fluorescence and phosphorescence peaks in neat methanol and in methanol mixed with acetonitrile are characteristic of Pt(pop)$^{4-}$. The control sample measured in acetonitrile maintains the signatures of Pt(pop-BF$_2$)$^{4-}$. In Pt(pop-BF$_2$)$^{4-}$ the fluorescence and phosphorescence emission peaks are nearly equal in intensity; in Pt(pop)$^{4-}$ the phosphorescence peak is ~40x more intense than the fluorescence peak. Accepted values for the emission maxima of Pt(pop)$^{4-}$ and Pt(pop-BF$_2$)$^{4-}$ are presented in Figure 10[2,4,17] together with the steady-state emission spectra of Pt(pop-BF$_2$)$^{4-}$ in the discussed solvent mixtures.

	λ_{max}, fluorescence	λ_{max}, phosphorescence
Pt(pop)$^{4-}$	398 nm	511 nm
Pt(pop-BF$_2$)$^{4-}$	393 nm	512 nm

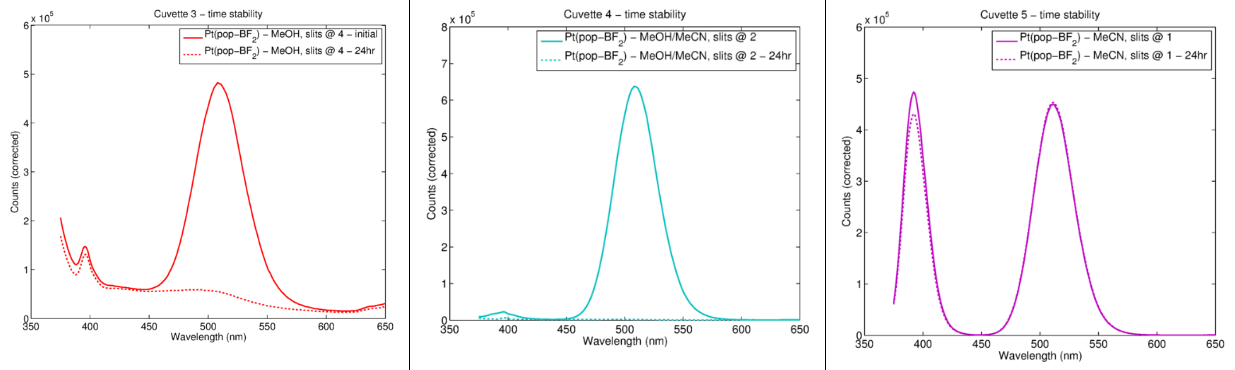

MeOH
$\lambda_{max,\,fl} = 396$ nm
$\lambda_{max,\,phos} = 509$ nm

MeOH/MeCN
$\lambda_{max,\,fl} = 396$ nm
$\lambda_{max,\,phos} = 509$ nm

MeCN
$\lambda_{max,\,fl} = 392$ nm
$\lambda_{max,\,phos} = 511$ nm

Figure 10: Steady-state emission spectra of Pt(pop-BF$_2$)$^{4-}$ in various solvents; decomposition to Pt(pop)$^{4-}$ noted in the presence of methanol.

Other solvents investigated for stability include 2-methyltetrahydrofuran (MeTHF), butyronitrile (BuCN), and propionitrile (PrCN); Pt(pop-BF$_2$)$^{4-}$ is soluble in BuCN and PrCN and sparingly soluble in MeTHF. Quantities of these three solvents were dried and purified.[16] However, Pt(pop-BF$_2$)$^{4-}$ proved to be unstable in a 1:1 mixture of MeCN:MeTHF (such a mixture was required for complete solubility) as noted by a significant decrease in both absorption intensity and singlet emission intensity during the course of a series of fluorimetry experiments.

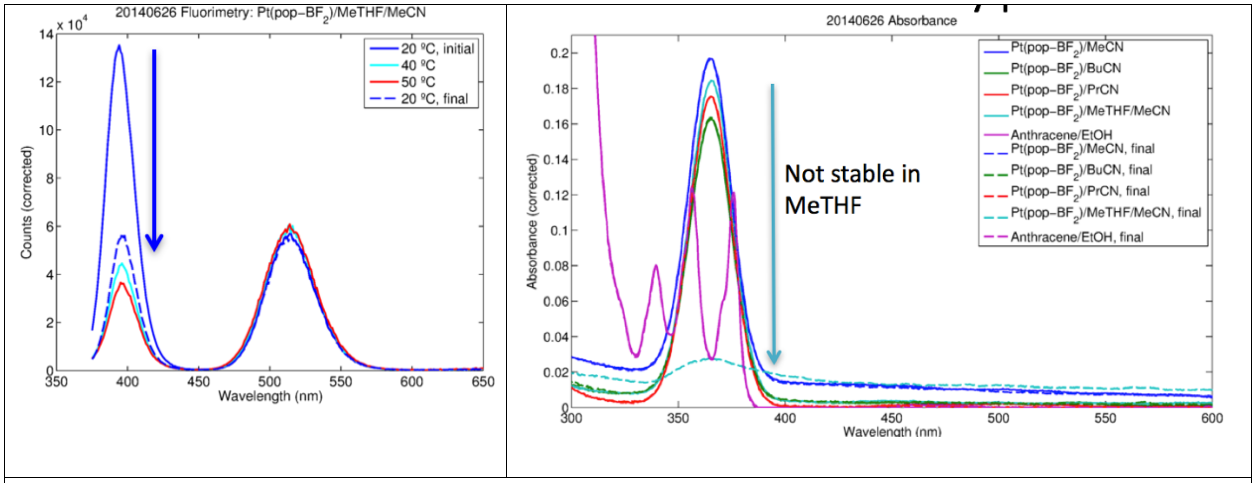

Figure 11: Decomposition of Pt(pop-BF$_2$)$^{4-}$ in MeCN/MeTHF during variable temperature fluorimetry experiments showing decrease in singlet emission intensity (left) with a concomintant decrease in absorption intensity (right).

While solutions of Pt(pop-BF$_2$)$^{4-}$ proved to be stable (as measured by absorption intensity) in BuCN and PrCN over temperatures ranging from 278 – 333 K for 48 hours (Figure 12), decomposition was noted following the laser measurements needed to obtain values for τ. This decomposition was noted both as a decrease in calculated quantum yield before and after the laser measurements due to overall decreases in luminescence intensity (Figure 13), as well as by decreases in absorption intensity (Figure 14). While the sample in MeCN also exhibited a decrease in luminescence intensity following the time-resolved laser experiments, the calculated quantum yield was the same; this indicates that the observed decrease for MeCN could be due to instrument fluctuation. However, the decreases observed for BuCN and PrCN solutions resulted in significantly different quantum yields, which shows that the change in intensity was not due to a systematic instrument error effective across all wavelengths. This is indicative of actual changes in the sample and cannot be attributed to instrument fluctuations. While during this experiment slightly longer lifetimes were observed in BuCN and PrCN as compared to MeCN, these data cannot be relied upon due to the sample decomposition.

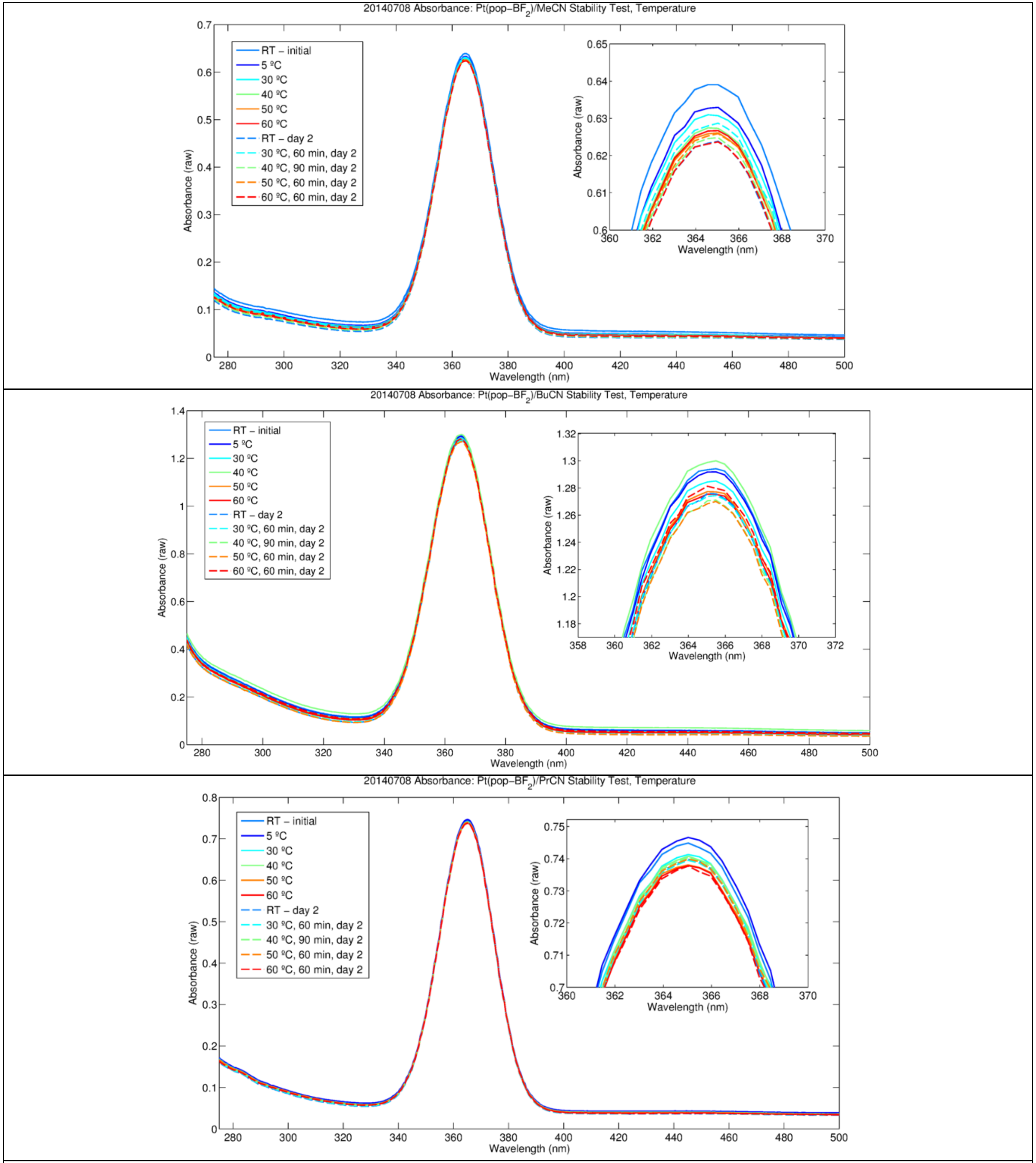

20140708 Absorbance: Pt(pop–BF$_2$)/MeCN Stability Test, Temperature

20140708 Absorbance: Pt(pop–BF$_2$)/BuCN Stability Test, Temperature

20140708 Absorbance: Pt(pop–BF$_2$)/PrCN Stability Test, Temperature

Figure 12: Absorption profile of $\mathrm{Pt(pop\text{-}BF_2)^{4-}}$ in MeCN (top), BuCN (middle), and PrCN(bottom) at temperatures from 278 – 333 K over 48 hours (day 1 values are solid lines; day 2 values are dashed lines). Insets show the region of maximum absorption.

	Φ_{fl}, initial, 20 ºC	Φ_{fl}, final, 20 ºC (after laser measurements)
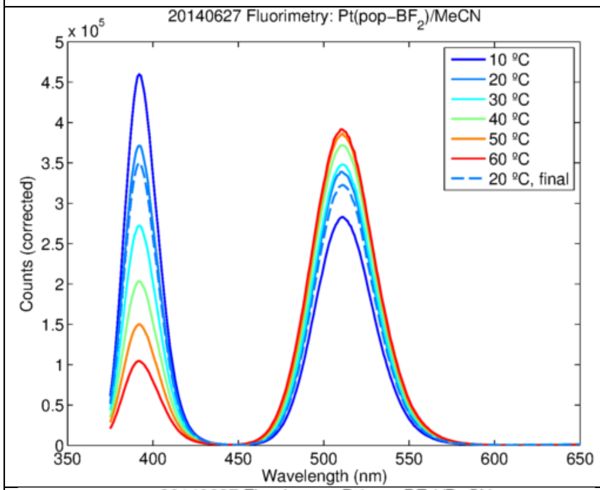 20140627 Fluorimetry: Pt(pop–BF$_2$)/MeCN	0.33	0.33
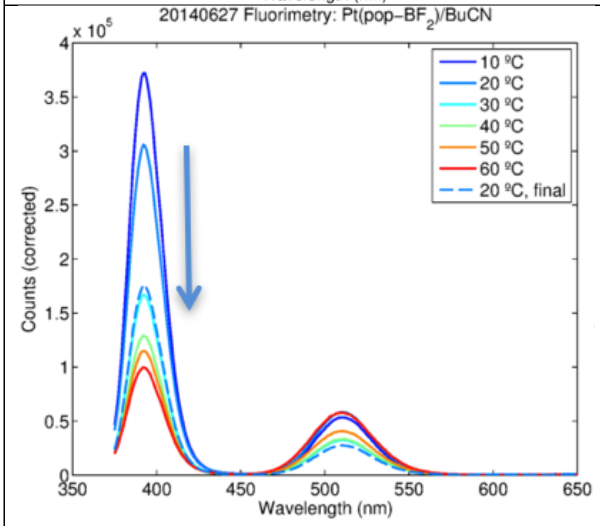 20140627 Fluorimetry: Pt(pop–BF$_2$)/BuCN	0.34	0.21
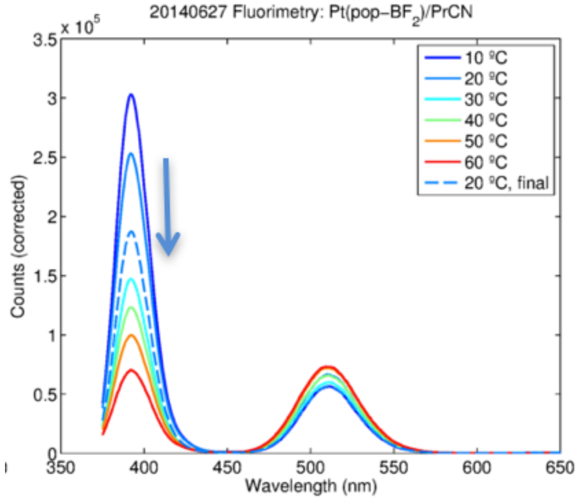 20140627 Fluorimetry: Pt(pop–BF$_2$)/PrCN	0.39	0.31

Figure 13: Decreases in luminescence intensity from before laser experiments (solid lines) to after (dashed lines), for solutions of Pt(pop-BF$_2$)$^{4-}$ in MeCN (top), BuCN (middle), and PrCN(bottom).

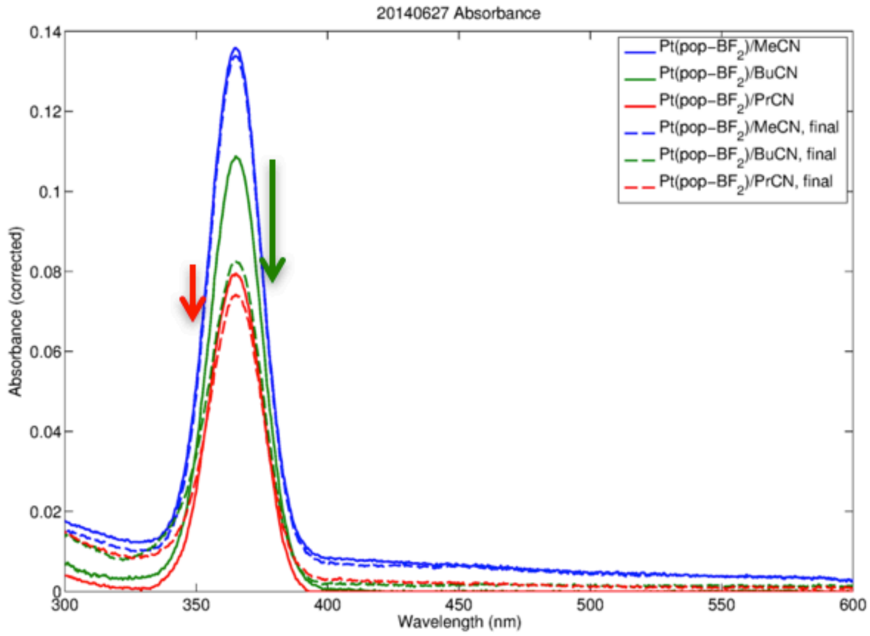

Figure 14: Changes in absorption intensity from before laser experiments (solid lines) to after (dashed lines), for solutions of Pt(pop-BF$_2$)$^{4-}$ in MeCN (blue), BuCN (green), and PrCN (red).

The noted sample decomposition can be attributed solely to laser exposure, as this experiment was repeated including every step except the time-resolved laser measurements. Absorption and luminescence profiles remained constant over the course of the steady-state fluorimetry measurements at temperatures from 293 to 333 K (Figure 15).

Steady-state luminescence spectra	Absorption spectra
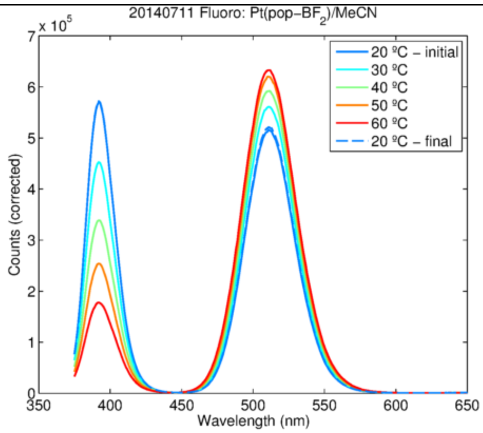	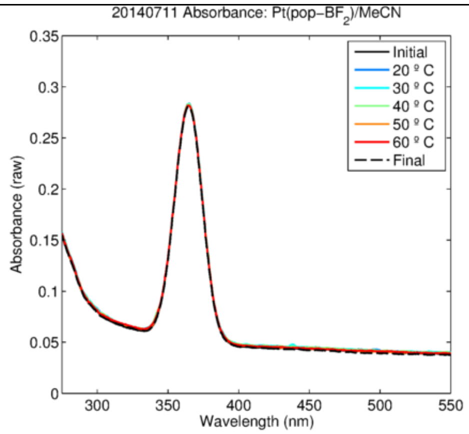
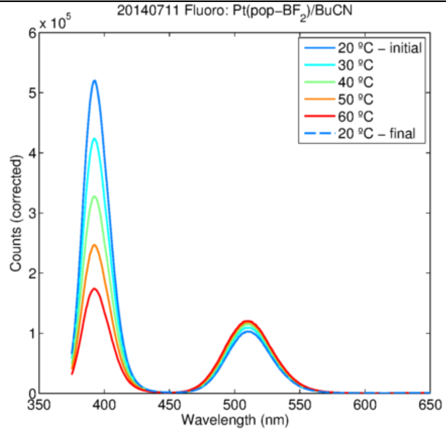	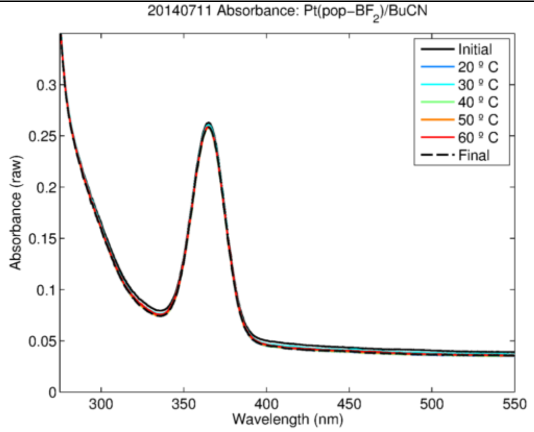
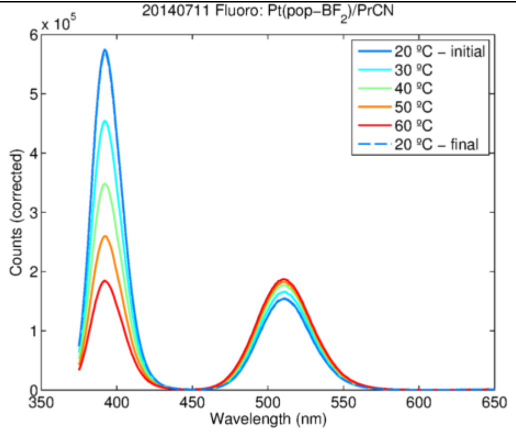	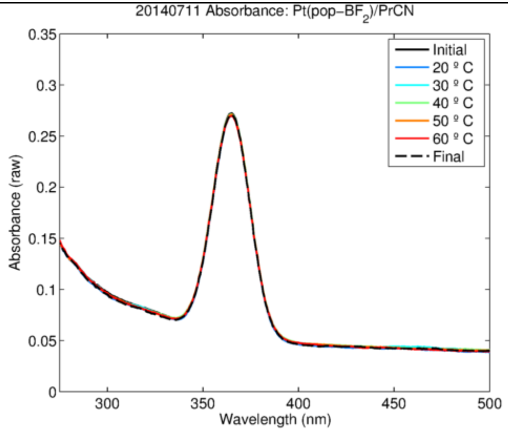

Figure 15: Temperature-dependent measurements excluding the time-resolved laser experimental portion indicates Pt(pop-BF$_2$)$^{4-}$ stability in MeCN (top), BuCN (middle), and PrCN (bottom).

2.4 Materials and methods

Unless otherwise noted, all reagents were obtained from Sigma-Aldrich and used without further purification; all water used was deionized. All manipulations involving Pt(pop-BF_2)$^{4-}$ were carried out with standard air-free techniques in an inert-atmosphere glovebox or by utilizing a vacuum manifold. Solvents were dried using activated alumina columns according to Grubbs' method.[18] Anhydrous acetonitrile was stored over activated 3 Å molecular sieves; all other anhydrous solvents were stored over activated 4 Å molecular sieves.[16] Molecular sieves were activated by heating to 200 ºC under reduced pressure for 4 hours.

2.4.1 *Phosphorous acid, H_3PO_3*

$$PCl_3 + 3\,H_2O \xrightarrow{CH_2Cl_2} H_3PO_3 + 3\,HCl$$

Phosphorous acid was prepared by adding 15.6 g phosphorus trichloride (PCl_3) to 40 mL dichloromethane in a round-bottom flask in an ice bath. 6 mL water was added to a dropping funnel and added to the stirring solution of PCl_3 over 30 minutes. The flask was removed from the ice bath and stirred at room temperature for 90 minutes. The dichloromethane was removed under reduced pressure and the remaining fluffy white solid was transferred to a vial and stored in a desiccator.

It is important to use a slight excess of PCl_3 in order to obtain a solid product. Excess water in the reaction will result in the formation of a thick, colorless oil; the H_3PO_3 product may be recovered from this oil via multiple solvent extractions using CH_2Cl_2.

The ^{31}P NMR exhibits a single peak at 5.86 ppm.

This reaction has been successfully scaled up to produce ~40 g of H_3PO_3 at a time; however, extreme care must be taken to add the water slowly to avoid dangerous exotherms. Furthermore, given the large amount of HCl gas produced at this scale, it is recommended to route the evolved gas through a bubbler filled with ice and an aqueous solution of either sodium bicarbonate or sodium hydroxide.

2.4.2 *$K_4Pt(pop)$*

$$2K_2PtCl_4 + 8\ H_3PO_3 \xrightarrow[100\ ^\circ C]{H_2O} K_4[Pt_2(P_2O_5H_2)_4] + 2\ H_2O + 8\ HCl$$

The water-soluble potassium salt of $Pt(pop)^{4-}$ was prepared by dissolving 0.326 g potassium tetrachloroplatinate (K_2PtCl_4) in 10 mL water. 1.48 g phosphorus acid (as prepared in 2.4.1) was dissolved in another 10 mL of water.[ii] The two solutions were mixed in a petri dish to give a light red solution; this was held over a boiling water bath for three hours to yield a lightly-colored yellow-brown solution. The petri dish was refilled with water every 30 minutes to maintain solution volume. The dish was transferred to a modified vacuum oven set to 110 ºC for three hours. This modified oven, rather than pulling vacuum, blew a constant stream of air through the oven to purge out evolved hydrochloric acid. The resulting bright yellow solid was suspended in methanol, isolated on a glass frit, and rinsed with copious methanol and diethyl ether. The isolated solid was collected and dried under vacuum. The isolated solid may range in color from bright yellowish-green to dark purple; when dissolved in water, the expected yellow-green

---

[ii] Commercially available phosphorous acid is often contaminated with water, as phosphorous acid is quite hygroscopic. Purchased phosphorous acid may be used for this synthesis, but yields may be adversely affected.

luminescent solution is reliably obtained. It has been proposed that the dark purple color is caused by a small amount of a highly colored impurity.[5]

^{31}P NMR exhibits a singlet at 67.1 ppm flanked by satellite peaks at 76.6 and 57.6 ppm caused by coupling to the compound’s ^{195}Pt atoms ($^1J_{Pt\text{-}P}$ = 3025 Hz, 33% abundance).

2.4.3 [TBA]$_4$[Pt(pop)]

$$K_4[Pt_2(P_2O_5H_2)_4] + 4\ [(n\text{-}Bu)_4N]Cl \xrightarrow{H_2O} [(n\text{-}Bu)_4N]_4[Pt_2(P_2O_5H_2)_4] + 4\ KCl$$

The tetrabutylammonium (TBA) salt of Pt(pop) was prepared by dissolving 0.35 g K$_4$[Pt(pop)] in 4 mL water. 2.5 g (a 30-fold excess) tetrabutylammonium chloride ([(n-Bu)$_4$N]Cl) was added to the solution and stirred for one hour at room temperature. In the dark, the syrupy aqueous solution was extracted with three 50 mL aliquots of dichloromethane and the organic layer was concentrated under vacuum to a volume of 5 mL. 50 mL ethyl acetate was added to induce precipitation of a bright yellow-green powder. The powder was isolated on a glass frit and dried under vacuum.

^{31}P NMR exhibits a single peak at 67.8 ppm flanked with the previously described ^{195}Pt coupling satellites. In the presence of light, Pt(pop)$^{4-}$ reacts with dichloromethane to form the chloride adduct, which exhibits a single peak at 30.1 ppm in the ^{31}P NMR spectrum.[19] The presence of this peak indicates a crude product which must be purified via recrystallization in the dark from a concentrated CH_2Cl_2 solution layered with ethyl acetate.

2.4.4 [Ph$_4$P]$_4$[Pt(pop)]

$$K_4[Pt_2(P_2O_5H_2)_4] + 4\ [Ph_4P]Cl \xrightarrow{H_2O} [Ph_4P]_4[Pt_2(P_2O_5H_2)_4] + 4\ KCl$$

The tetraphenylphosphonium (Ph_4P^+) salt of $Pt(pop)^{4-}$ may be prepared by a similar salt metathesis procedure to that described in 2.4.3. Briefly, 1.2 g Ph_4PCl was dissolved in 20 mL water and 0.28 g $K_4Pt(pop)$ was dissolved in 50 mL water; both solutions were sparged with nitrogen for 15 minutes. The tetraphenylphosphonium chloride solution was then added to the $Pt(pop)^{4-}$ solution and a light yellow solid precipitated immediately. The solid was isolated via vacuum filtration through fine glass-fiber filter paper and dried under vacuum.

Crystals suitable for X-ray diffraction analysis (bright yellow-green needles) were grown from slow evaporation of a dilute methanol solution of the product. The ^{31}P NMR exhibited a single peak at 66.83 ppm, flanked by the previously discussed ^{195}Pt satellite peaks.

2.4.5 $[Ph_4As]_4[Pt(pop)]$

The tetraphenylarsonium (Ph_4As^+) salt of $Pt(pop)^{4-}$ may be prepared in a similar salt metathesis procedure to that described in 2.4.4. Briefly, 0.93 g Ph_4AsCl was dissolved in 20 mL water and 0.34 g $K_4Pt(pop)$ was dissolved in 50 mL water; both solutions were sparged with nitrogen for 15 minutes. The tetraphenylphosphonium solution was then added to the $Pt(pop)^{4-}$ solution and a light yellow solid precipitated immediately. The solid was isolated via vacuum filtration through fine glass-fiber filter paper and dried under vacuum.

The ^{31}P NMR exhibited a single peak at 67.1 ppm, flanked by the previously discussed ^{195}Pt satellite peaks.

2.4.6 $[Pt(pop\text{-}BF_2)]^{4-}$

$$[R]_4[Pt_2(P_2O_5H_2)_4] + BF_3{\bullet}Et_2O \longrightarrow [R]_4[Pt_2(P_2O_5B_2F_4)_4] + HF$$

$$R = (n\text{-}Bu)_4N^+,\ Ph_4P^+,\ Ph_4As^+$$

$[R]_4[Pt(pop\text{-}BF_2)]$, where R = Ph_4P^+, $(n\text{-}Bu)_4N^+$, or Ph_4As^+, was prepared by adding 0.3 – 0.6 g of the appropriate $Pt(pop)^{4-}$ salt to a 10 mL Schlenk flask. After sparging with dry argon for 15 minutes, a syringe was used to add 3.5 mL boron trifluoride diethyletherate ($BF_3{\bullet}Et_2O$) to the flask through a rubber septum. Under positive argon flow, the rubber septum was replaced with a ground-glass stopper; the reaction was then left stirring under a static blanket of argon for six hours (although the reaction may be left stirring for multiple days with no decomposition). The remaining $BF_3{\bullet}Et_2O$ was removed under reduced pressure in a 40 ºC water bath. The $BF_3{\bullet}Et_2O$ was condensed into an ice-cooled pre-trap immediately in line after the Schlenk flask. If a pre-trap is not used, $BF_3{\bullet}Et_2O$ will condense inside the vacuum tubing and/or the Schlenk line itself, causing contamination and presenting a significant health and safety hazard to researchers. Removal of solvent yielded a bright yellow-green powder. The Schlenk flask containing the product was sealed under nitrogen and taken into an inert-atmosphere glovebox; the product was then suspended in dry tetrahydrofuran (THF), filtered through a glass frit, and rinsed with copious THF. The isolated product was dried under vacuum and recrystallized via slow evaporation of diethylether into a saturated acetonitrile solution to yield bright yellow-green luminescent crystalline blocks.

The ^{31}P NMR exhibits a single peak at ≈58.8 ppm (depending on the cation; see section 2.5) together with the aforementioned ^{195}Pt coupling satellite peaks ($^1J_{Pt\text{-}P} \cong$ 3126 – 3136 Hz). The ^{19}F NMR exhibits two doublets at 133.5 ppm (^1J = 60 Hz) and 138.7 ppm (^1J = 60 Hz).

2.4.7 X-ray structure determination of $[Ph_4P]_4[Pt(pop\text{-}BF_2)]$

Low-temperature diffraction data (ϕ-and ω-scans) were collected on a Bruker three-circle diffractometer coupled to a Bruker Smart 1000 CCD detector with graphite monochromated Mo

K_α radiation (λ = 0.71073 Å) for the structure of $[Ph_4P]_4[Pt(pop\text{-}BF_2)]$. The structure was solved by direct methods using SHELXS[20] and refined against F^2 on all data by full-matrix least squares with SHELXL-2013[21] using established refinement techniques.[22] All non-hydrogen atoms were refined anisotropically. All hydrogen atoms were included into the model at geometrically calculated positions and refined using a riding model. The isotropic displacement parameters of all hydrogen atoms were fixed to 1.2 times the U value of the atoms they are linked to (1.5 times for methyl groups). Data are presented in section 2.6.

2.4.8 *Steady-state quenching experiments*

Steady-state emission spectra were recorded on a Jobin Yvon Spex Fluorolog-3-11. A 450-W xenon arc lamp was used as the excitation source with a single monochromator providing wavelength selection. Right-angle light emission was sorted using a single monochromator and fed into a Hamamatsu R928P photomultiplier tube with photon counting. Short and long pass filters were used where appropriate. Spectra were recorded on Datamax software.[2] Variable-temperature experiments were performed using a Peltier-cooled circulating water bath.

2.4.9 *Temperature-dependent lifetime experiments: Picosecond laser data*[2]

An IBH 5000 U instrument equipped with a cooled Hamamatsu R3809U-50 microchannel plate photomultiplier was used. Samples were excited at 355 nm with an IBH NanoLED-03 diode laser (~80 ps fwhm, repetition rate 500 kHz). For fluorescence decay measurements, the emission monochromator was set to ≈405 ± 4 nm, preceded by a 390 nm long-pass cutoff filter to remove stray excitation light. Magic angle between the excitation and emission polarization directions was used for all experiments. Variable-temperature experiments were performed using a Peltier-cooled circulating water bath. Data manipulation was performed and plotted using MATLAB R2015a (Mathworks, Inc.).

2.5 NMR spectra

All NMR spectra were recorded in the Caltech Liquid NMR facility using a Varian 400 MHz spectrometer with a broadband auto-tune OneProbe ("Siena"). All ^{31}P spectra were externally referenced to 85% phosphoric acid. Spectra were processed using the MestReNova software suite.[23]

<table>
<tr><th colspan="2">K$_4$Pt(pop)</th></tr>
<tr><td>^{1}H</td><td>^{31}P</td></tr>
<tr><td>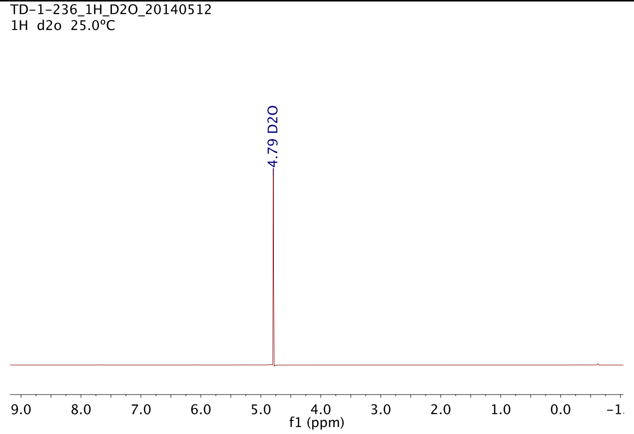
</td><td>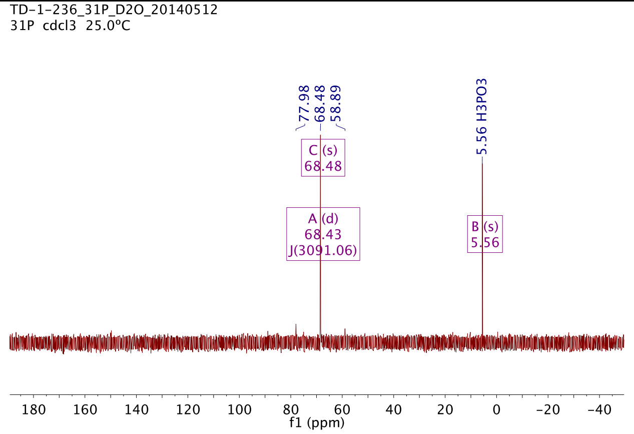
</td></tr>
<tr><th colspan="2">[(n-Bu)$_4$P]$_4$[Pt(pop-BF$_2$)]</th></tr>
<tr><td>^{1}H</td><td>^{31}P</td></tr>
</table>

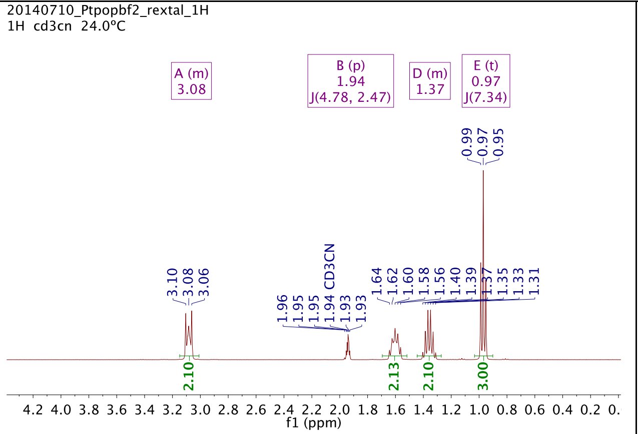

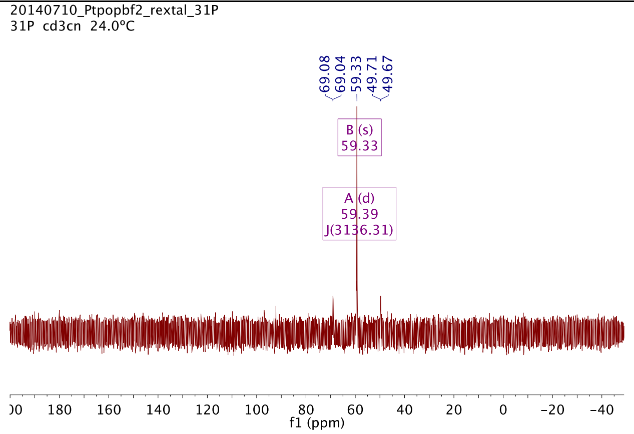

^{19}F

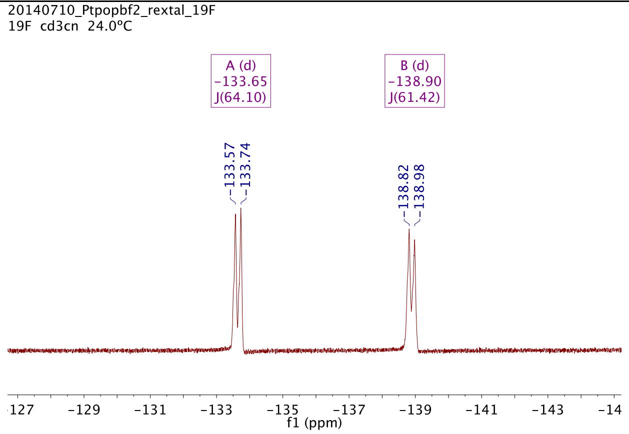

$[Ph_4P]_4[Pt(pop\text{-}BF_2)]$

^{1}H

^{31}P

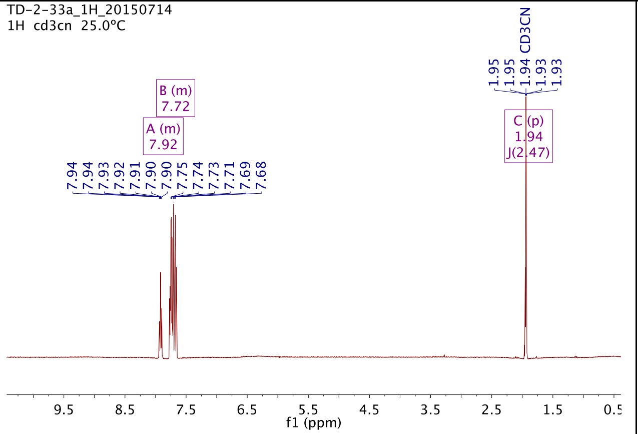

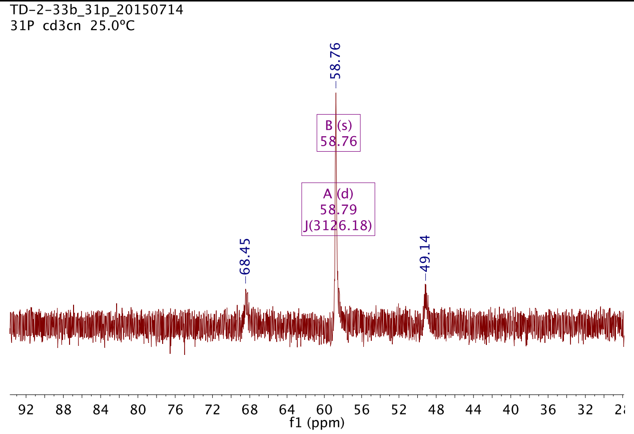

^{19}F

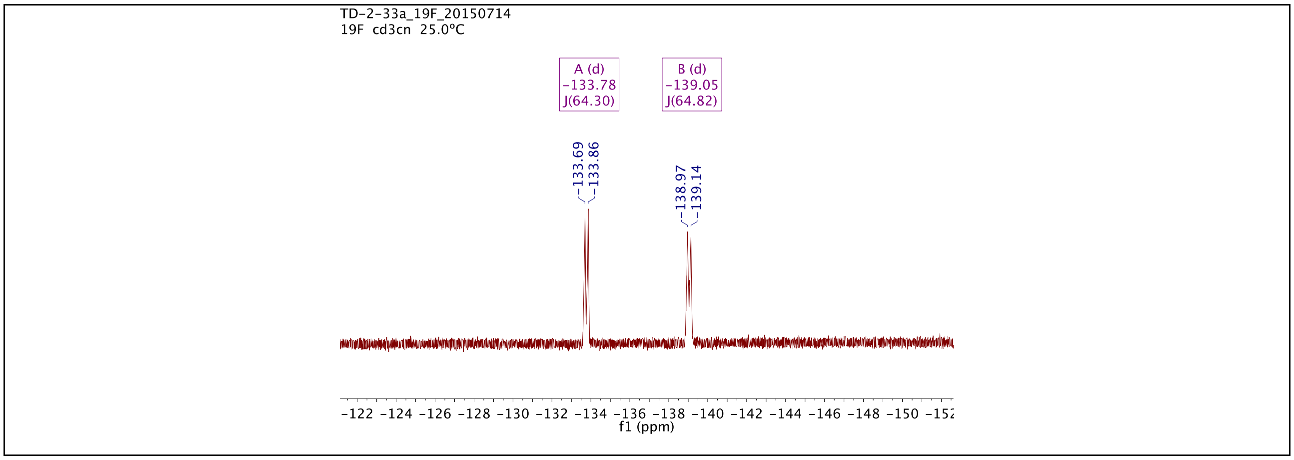

2.6 X-ray data for $[Ph_4P]_4[Pt(pop\text{-}BF_2)]$

Table 1: Crystal data and structure refinement for S13045.

Identification code	S13045	
Empirical formula	C96 H80 B8 F16 O20 P12 Pt2	
Formula weight	2705.90	
Temperature	100(2) K	
Wavelength	0.71073 Å	
Crystal system	Monoclinic	
Space group	P 21/n	
Unit cell dimensions	a = 15.8751(6) Å	a= 90°.
	b = 17.2490(6) Å	b= 98.5184(18)°.
	c = 18.6455(7) Å	g = 90°.
Volume	5049.4(3) $Å^3$	
Z	2	
Density (calculated)	1.780 Mg/m^3	
Absorption coefficient	3.058 mm^{-1}	
F(000)	2672	
Crystal size	0.400 x 0.300 x 0.300 mm^3	
Theta range for data collection	1.617 to 36.377°.	
Index ranges	-26<=h<=26, -28<=k<=28, -31<=l<=30	
Reflections collected	149401	
Independent reflections	24436 [R(int) = 0.0435]	
Completeness to theta = 25.242°	100.0 %	

Absorption correction	Semi-empirical from equivalents
Max. and min. transmission	0.7471 and 0.4555
Refinement method	Full-matrix least-squares on F^2
Data / restraints / parameters	24436 / 0 / 694
Goodness-of-fit on F^2	1.098
Final R indices [I>2sigma(I)]	R1 = 0.0329, wR2 = 0.0745
R indices (all data)	R1 = 0.0502, wR2 = 0.0843
Extinction coefficient	n/a
Largest diff. peak and hole	4.106 and -1.695 e.Å^{-3}

Table 2: Atomic coordinates (x 10^4) and equivalent isotropic displacement parameters (Å^{2}x 10^3) for S13045. U(eq) is defined as one third of the trace of the orthogonalized U^{ij} tensor.

	x	y	z	U(eq)
Pt(1)	9405(1)	5584(1)	5154(1)	10(1)
P(1)	10469(1)	6423(1)	5622(1)	13(1)
O(1)	10476(1)	6693(1)	6409(1)	20(1)
B(1)	9955(2)	6477(2)	6981(2)	18(1)
F(1)	10439(1)	6602(1)	7643(1)	29(1)
F(2)	9224(1)	6917(1)	6894(1)	36(1)
O(2)	9723(1)	5642(1)	6933(1)	25(1)
P(2)	9395(1)	5106(1)	6298(1)	12(1)
O(3)	8546(1)	4766(1)	6459(1)	20(1)
B(2)	7701(2)	4764(2)	5989(1)	17(1)
F(3)	7387(1)	5517(1)	5925(1)	26(1)
F(4)	7180(1)	4280(1)	6308(1)	25(1)
O(4)	7765(1)	4454(1)	5260(1)	16(1)
O(5)	8616(1)	3990(1)	4344(1)	19(1)
P(3)	8305(1)	4772(1)	4700(1)	11(1)
O(6)	7664(1)	5131(1)	4091(1)	17(1)
B(3)	7778(2)	5571(2)	3428(1)	21(1)
F(5)	7048(1)	5986(2)	3220(1)	48(1)

F(6)	7936(2)	5054(1)	2905(1)	53(1)
O(7)	8499(1)	6125(1)	3550(1)	18(1)
O(8)	9968(1)	5623(1)	3541(1)	22(1)
P(4)	9377(1)	6106(1)	4018(1)	12(1)
O(9)	9694(1)	6949(1)	3993(1)	21(1)
B(4)	10448(2)	7337(2)	4408(2)	20(1)
F(7)	10361(1)	8113(1)	4301(1)	40(1)
F(8)	11185(1)	7060(2)	4179(1)	40(1)
O(10)	10521(1)	7184(1)	5200(1)	21(1)
P(5)	9558(1)	8187(1)	1153(1)	15(1)
C(1)	8687(1)	7969(1)	1629(1)	17(1)
C(2)	8310(2)	8544(2)	2001(2)	24(1)
C(3)	7631(2)	8345(2)	2358(2)	31(1)
C(4)	7350(2)	7588(2)	2365(2)	26(1)
C(5)	7729(2)	7018(2)	1999(2)	22(1)
C(6)	8392(2)	7207(2)	1620(1)	21(1)
C(11)	10533(1)	7784(1)	1620(1)	16(1)
C(12)	10527(2)	7269(1)	2200(1)	18(1)
C(13)	11292(2)	6954(2)	2543(1)	21(1)
C(14)	12055(2)	7155(2)	2317(1)	22(1)
C(15)	12068(2)	7682(2)	1749(1)	21(1)
C(16)	11310(2)	7994(2)	1402(1)	19(1)
C(21)	9306(2)	7764(1)	264(1)	17(1)
C(22)	9926(2)	7397(2)	-79(1)	20(1)
C(23)	9702(2)	7082(2)	-768(1)	23(1)
C(24)	8865(2)	7133(2)	-1117(2)	25(1)
C(25)	8250(2)	7498(2)	-781(2)	26(1)
C(26)	8465(2)	7814(2)	-90(1)	21(1)
C(31)	9693(2)	9215(1)	1105(1)	17(1)
C(32)	9219(2)	9643(2)	548(1)	21(1)
C(33)	9288(2)	10448(2)	554(2)	26(1)
C(34)	9826(2)	10823(2)	1099(2)	29(1)
C(35)	10305(2)	10396(2)	1648(2)	28(1)
C(36)	10234(2)	9595(2)	1658(2)	24(1)
P(6)	7680(1)	9757(1)	4861(1)	15(1)
C(41)	8545(2)	10091(2)	4419(1)	19(1)

C(42)	8629(2)	10881(2)	4280(1)	23(1)
C(43)	9257(2)	11132(2)	3887(2)	28(1)
C(44)	9784(2)	10592(2)	3621(2)	32(1)
C(45)	9701(2)	9805(2)	3756(2)	33(1)
C(46)	9083(2)	9548(2)	4159(2)	26(1)
C(51)	6716(2)	10144(1)	4372(1)	17(1)
C(52)	6605(2)	10098(2)	3615(1)	21(1)
C(53)	5825(2)	10283(2)	3221(2)	28(1)
C(54)	5159(2)	10521(2)	3572(2)	29(1)
C(55)	5279(2)	10601(2)	4320(2)	26(1)
C(56)	6060(2)	10413(2)	4726(2)	21(1)
C(61)	7626(2)	8717(1)	4825(1)	18(1)
C(62)	7022(2)	8336(2)	4327(1)	21(1)
C(63)	6999(2)	7528(2)	4315(2)	27(1)
C(64)	7577(2)	7108(2)	4794(2)	30(1)
C(65)	8185(2)	7485(2)	5282(2)	31(1)
C(66)	8219(2)	8283(2)	5299(2)	26(1)
C(71)	7756(2)	10051(1)	5791(1)	17(1)
C(72)	7326(2)	9619(2)	6261(1)	22(1)
C(73)	7305(2)	9880(2)	6962(1)	25(1)
C(74)	7704(2)	10571(2)	7195(1)	23(1)
C(75)	8134(2)	10996(2)	6733(1)	22(1)
C(76)	8162(2)	10743(2)	6028(1)	19(1)

Table 3: Bond lengths [Å] and angles [°] for S13045.

Pt(1)-P(2)	2.2880(6)
Pt(1)-P(1)	2.2958(5)
Pt(1)-P(4)	2.2966(6)
Pt(1)-P(3)	2.3003(5)
Pt(1)-Pt(1)#1	2.87596(16)
P(1)-O(1)	1.5376(18)
P(1)-O(10)	1.5400(19)

P(1)-O(5)#1	1.6110(18)
O(1)-B(1)	1.490(3)
B(1)-F(1)	1.371(3)
B(1)-F(2)	1.377(3)
B(1)-O(2)	1.486(3)
O(2)-P(2)	1.5318(18)
P(2)-O(3)	1.5392(18)
P(2)-O(8)#1	1.6145(18)
O(3)-B(2)	1.491(3)
B(2)-F(4)	1.372(3)
B(2)-F(3)	1.388(3)
B(2)-O(4)	1.478(3)
O(4)-P(3)	1.5453(17)
O(5)-P(1)#1	1.6110(18)
O(5)-P(3)	1.6134(18)
P(3)-O(6)	1.5389(17)
O(6)-B(3)	1.483(3)
B(3)-F(5)	1.368(4)
B(3)-F(6)	1.373(4)
B(3)-O(7)	1.483(3)
O(7)-P(4)	1.5308(17)
O(8)-P(2)#1	1.6146(18)
O(8)-P(4)	1.6156(19)
P(4)-O(9)	1.5431(18)
O(9)-B(4)	1.485(3)
B(4)-F(7)	1.357(3)
B(4)-F(8)	1.388(4)
B(4)-O(10)	1.487(3)
P(5)-C(31)	1.789(2)
P(5)-C(1)	1.791(2)
P(5)-C(11)	1.799(2)
P(5)-C(21)	1.801(2)
C(1)-C(6)	1.395(3)
C(1)-C(2)	1.395(3)
C(2)-C(3)	1.390(4)
C(2)-H(2)	0.9500

C(3)-C(4)	1.381(4)
C(3)-H(3)	0.9500
C(4)-C(5)	1.383(4)
C(4)-H(4)	0.9500
C(5)-C(6)	1.391(3)
C(5)-H(5)	0.9500
C(6)-H(6)	0.9500
C(11)-C(12)	1.401(3)
C(11)-C(16)	1.402(3)
C(12)-C(13)	1.396(3)
C(12)-H(12)	0.9500
C(13)-C(14)	1.384(4)
C(13)-H(13)	0.9500
C(14)-C(15)	1.398(4)
C(14)-H(14)	0.9500
C(15)-C(16)	1.388(3)
C(15)-H(15)	0.9500
C(16)-H(16)	0.9500
C(21)-C(22)	1.402(3)
C(21)-C(26)	1.403(3)
C(22)-C(23)	1.391(4)
C(22)-H(22)	0.9500
C(23)-C(24)	1.394(4)
C(23)-H(23)	0.9500
C(24)-C(25)	1.386(4)
C(24)-H(24)	0.9500
C(25)-C(26)	1.393(4)
C(25)-H(25)	0.9500
C(26)-H(26)	0.9500
C(31)-C(32)	1.400(3)
C(31)-C(36)	1.403(4)
C(32)-C(33)	1.393(4)
C(32)-H(32)	0.9500
C(33)-C(34)	1.387(4)
C(33)-H(33)	0.9500
C(34)-C(35)	1.392(4)

C(34)-H(34)	0.9500
C(35)-C(36)	1.388(4)
C(35)-H(35)	0.9500
C(36)-H(36)	0.9500
P(6)-C(51)	1.791(2)
P(6)-C(71)	1.793(2)
P(6)-C(61)	1.797(3)
P(6)-C(41)	1.797(3)
C(41)-C(42)	1.398(4)
C(41)-C(46)	1.401(4)
C(42)-C(43)	1.390(4)
C(42)-H(42)	0.9500
C(43)-C(44)	1.391(5)
C(43)-H(43)	0.9500
C(44)-C(45)	1.390(5)
C(44)-H(44)	0.9500
C(45)-C(46)	1.393(4)
C(45)-H(45)	0.9500
C(46)-H(46)	0.9500
C(51)-C(56)	1.393(3)
C(51)-C(52)	1.399(3)
C(52)-C(53)	1.381(4)
C(52)-H(52)	0.9500
C(53)-C(54)	1.385(5)
C(53)-H(53)	0.9500
C(54)-C(55)	1.385(4)
C(54)-H(54)	0.9500
C(55)-C(56)	1.392(4)
C(55)-H(55)	0.9500
C(56)-H(56)	0.9500
C(61)-C(62)	1.396(3)
C(61)-C(66)	1.407(4)
C(62)-C(63)	1.395(4)
C(62)-H(62)	0.9500
C(63)-C(64)	1.387(4)
C(63)-H(63)	0.9500

C(64)-C(65)	1.385(5)
C(64)-H(64)	0.9500
C(65)-C(66)	1.379(4)
C(65)-H(65)	0.9500
C(66)-H(66)	0.9500
C(71)-C(76)	1.397(3)
C(71)-C(72)	1.402(3)
C(72)-C(73)	1.388(4)
C(72)-H(72)	0.9500
C(73)-C(74)	1.389(4)
C(73)-H(73)	0.9500
C(74)-C(75)	1.384(4)
C(74)-H(74)	0.9500
C(75)-C(76)	1.392(3)
C(75)-H(75)	0.9500
C(76)-H(76)	0.9500

P(2)-Pt(1)-P(1)	88.81(2)
P(2)-Pt(1)-P(4)	177.48(2)
P(1)-Pt(1)-P(4)	90.95(2)
P(2)-Pt(1)-P(3)	90.79(2)
P(1)-Pt(1)-P(3)	177.92(2)
P(4)-Pt(1)-P(3)	89.368(19)
P(2)-Pt(1)-Pt(1)#1	91.728(15)
P(1)-Pt(1)-Pt(1)#1	92.871(15)
P(4)-Pt(1)-Pt(1)#1	90.787(15)
P(3)-Pt(1)-Pt(1)#1	89.183(14)
O(1)-P(1)-O(10)	103.68(11)
O(1)-P(1)-O(5)#1	102.59(10)
O(10)-P(1)-O(5)#1	106.25(11)
O(1)-P(1)-Pt(1)	117.06(7)
O(10)-P(1)-Pt(1)	115.83(7)
O(5)#1-P(1)-Pt(1)	110.13(7)
B(1)-O(1)-P(1)	132.87(16)
F(1)-B(1)-F(2)	111.7(2)
F(1)-B(1)-O(2)	107.9(2)

F(2)-B(1)-O(2)	109.3(2)
F(1)-B(1)-O(1)	108.0(2)
F(2)-B(1)-O(1)	108.9(2)
O(2)-B(1)-O(1)	111.0(2)
B(1)-O(2)-P(2)	133.14(17)
O(2)-P(2)-O(3)	106.65(11)
O(2)-P(2)-O(8)#1	101.19(12)
O(3)-P(2)-O(8)#1	102.03(11)
O(2)-P(2)-Pt(1)	117.08(8)
O(3)-P(2)-Pt(1)	116.54(7)
O(8)#1-P(2)-Pt(1)	111.28(7)
B(2)-O(3)-P(2)	128.56(15)
F(4)-B(2)-F(3)	112.1(2)
F(4)-B(2)-O(4)	107.8(2)
F(3)-B(2)-O(4)	109.4(2)
F(4)-B(2)-O(3)	107.02(19)
F(3)-B(2)-O(3)	109.2(2)
O(4)-B(2)-O(3)	111.26(18)
B(2)-O(4)-P(3)	127.80(15)
P(1)#1-O(5)-P(3)	133.11(11)
O(6)-P(3)-O(4)	105.61(9)
O(6)-P(3)-O(5)	104.04(10)
O(4)-P(3)-O(5)	102.45(10)
O(6)-P(3)-Pt(1)	114.17(7)
O(4)-P(3)-Pt(1)	115.76(7)
O(5)-P(3)-Pt(1)	113.45(6)
B(3)-O(6)-P(3)	132.22(16)
F(5)-B(3)-F(6)	111.9(3)
F(5)-B(3)-O(6)	107.5(2)
F(6)-B(3)-O(6)	108.6(2)
F(5)-B(3)-O(7)	108.0(2)
F(6)-B(3)-O(7)	108.0(2)
O(6)-B(3)-O(7)	112.89(19)
B(3)-O(7)-P(4)	133.61(16)
P(2)#1-O(8)-P(4)	134.28(12)
O(7)-P(4)-O(9)	103.65(10)

O(7)-P(4)-O(8)	104.57(10)
O(9)-P(4)-O(8)	104.47(11)
O(7)-P(4)-Pt(1)	115.25(7)
O(9)-P(4)-Pt(1)	115.83(7)
O(8)-P(4)-Pt(1)	111.83(7)
B(4)-O(9)-P(4)	130.59(17)
F(7)-B(4)-F(8)	111.5(2)
F(7)-B(4)-O(9)	108.1(2)
F(8)-B(4)-O(9)	109.6(2)
F(7)-B(4)-O(10)	108.1(2)
F(8)-B(4)-O(10)	107.4(2)
O(9)-B(4)-O(10)	112.1(2)
B(4)-O(10)-P(1)	131.03(16)
C(31)-P(5)-C(1)	109.89(11)
C(31)-P(5)-C(11)	107.84(11)
C(1)-P(5)-C(11)	110.57(11)
C(31)-P(5)-C(21)	111.49(11)
C(1)-P(5)-C(21)	106.81(11)
C(11)-P(5)-C(21)	110.26(11)
C(6)-C(1)-C(2)	120.6(2)
C(6)-C(1)-P(5)	118.29(18)
C(2)-C(1)-P(5)	121.14(19)
C(3)-C(2)-C(1)	118.8(3)
C(3)-C(2)-H(2)	120.6
C(1)-C(2)-H(2)	120.6
C(4)-C(3)-C(2)	120.8(3)
C(4)-C(3)-H(3)	119.6
C(2)-C(3)-H(3)	119.6
C(3)-C(4)-C(5)	120.2(3)
C(3)-C(4)-H(4)	119.9
C(5)-C(4)-H(4)	119.9
C(4)-C(5)-C(6)	120.1(3)
C(4)-C(5)-H(5)	120.0
C(6)-C(5)-H(5)	120.0
C(5)-C(6)-C(1)	119.5(2)
C(5)-C(6)-H(6)	120.3

C(1)-C(6)-H(6)	120.3
C(12)-C(11)-C(16)	119.6(2)
C(12)-C(11)-P(5)	121.00(18)
C(16)-C(11)-P(5)	119.36(18)
C(13)-C(12)-C(11)	119.7(2)
C(13)-C(12)-H(12)	120.1
C(11)-C(12)-H(12)	120.1
C(14)-C(13)-C(12)	120.3(2)
C(14)-C(13)-H(13)	119.9
C(12)-C(13)-H(13)	119.9
C(13)-C(14)-C(15)	120.4(2)
C(13)-C(14)-H(14)	119.8
C(15)-C(14)-H(14)	119.8
C(16)-C(15)-C(14)	119.7(2)
C(16)-C(15)-H(15)	120.1
C(14)-C(15)-H(15)	120.1
C(15)-C(16)-C(11)	120.2(2)
C(15)-C(16)-H(16)	119.9
C(11)-C(16)-H(16)	119.9
C(22)-C(21)-C(26)	119.8(2)
C(22)-C(21)-P(5)	121.85(18)
C(26)-C(21)-P(5)	118.36(19)
C(23)-C(22)-C(21)	119.7(2)
C(23)-C(22)-H(22)	120.1
C(21)-C(22)-H(22)	120.1
C(22)-C(23)-C(24)	120.2(2)
C(22)-C(23)-H(23)	119.9
C(24)-C(23)-H(23)	119.9
C(25)-C(24)-C(23)	120.3(2)
C(25)-C(24)-H(24)	119.8
C(23)-C(24)-H(24)	119.8
C(24)-C(25)-C(26)	120.2(2)
C(24)-C(25)-H(25)	119.9
C(26)-C(25)-H(25)	119.9
C(25)-C(26)-C(21)	119.8(2)
C(25)-C(26)-H(26)	120.1

C(21)-C(26)-H(26)	120.1
C(32)-C(31)-C(36)	120.1(2)
C(32)-C(31)-P(5)	120.34(19)
C(36)-C(31)-P(5)	119.37(19)
C(33)-C(32)-C(31)	119.2(3)
C(33)-C(32)-H(32)	120.4
C(31)-C(32)-H(32)	120.4
C(34)-C(33)-C(32)	120.7(3)
C(34)-C(33)-H(33)	119.7
C(32)-C(33)-H(33)	119.7
C(33)-C(34)-C(35)	120.2(3)
C(33)-C(34)-H(34)	119.9
C(35)-C(34)-H(34)	119.9
C(36)-C(35)-C(34)	120.0(3)
C(36)-C(35)-H(35)	120.0
C(34)-C(35)-H(35)	120.0
C(35)-C(36)-C(31)	119.9(3)
C(35)-C(36)-H(36)	120.1
C(31)-C(36)-H(36)	120.1
C(51)-P(6)-C(71)	108.47(11)
C(51)-P(6)-C(61)	108.71(11)
C(71)-P(6)-C(61)	108.29(11)
C(51)-P(6)-C(41)	107.51(11)
C(71)-P(6)-C(41)	113.97(11)
C(61)-P(6)-C(41)	109.77(12)
C(42)-C(41)-C(46)	120.4(2)
C(42)-C(41)-P(6)	119.87(19)
C(46)-C(41)-P(6)	119.4(2)
C(43)-C(42)-C(41)	119.8(3)
C(43)-C(42)-H(42)	120.1
C(41)-C(42)-H(42)	120.1
C(42)-C(43)-C(44)	119.7(3)
C(42)-C(43)-H(43)	120.1
C(44)-C(43)-H(43)	120.1
C(45)-C(44)-C(43)	120.7(3)
C(45)-C(44)-H(44)	119.6

C(43)-C(44)-H(44)	119.6
C(44)-C(45)-C(46)	120.1(3)
C(44)-C(45)-H(45)	120.0
C(46)-C(45)-H(45)	120.0
C(45)-C(46)-C(41)	119.2(3)
C(45)-C(46)-H(46)	120.4
C(41)-C(46)-H(46)	120.4
C(56)-C(51)-C(52)	120.4(2)
C(56)-C(51)-P(6)	121.73(18)
C(52)-C(51)-P(6)	117.56(19)
C(53)-C(52)-C(51)	119.5(3)
C(53)-C(52)-H(52)	120.3
C(51)-C(52)-H(52)	120.3
C(52)-C(53)-C(54)	120.3(3)
C(52)-C(53)-H(53)	119.8
C(54)-C(53)-H(53)	119.8
C(53)-C(54)-C(55)	120.2(2)
C(53)-C(54)-H(54)	119.9
C(55)-C(54)-H(54)	119.9
C(54)-C(55)-C(56)	120.3(3)
C(54)-C(55)-H(55)	119.9
C(56)-C(55)-H(55)	119.9
C(55)-C(56)-C(51)	119.2(2)
C(55)-C(56)-H(56)	120.4
C(51)-C(56)-H(56)	120.4
C(62)-C(61)-C(66)	119.8(2)
C(62)-C(61)-P(6)	121.26(19)
C(66)-C(61)-P(6)	118.9(2)
C(63)-C(62)-C(61)	119.7(3)
C(63)-C(62)-H(62)	120.2
C(61)-C(62)-H(62)	120.2
C(64)-C(63)-C(62)	119.9(3)
C(64)-C(63)-H(63)	120.1
C(62)-C(63)-H(63)	120.1
C(65)-C(64)-C(63)	120.6(3)
C(65)-C(64)-H(64)	119.7

C(63)-C(64)-H(64)	119.7
C(66)-C(65)-C(64)	120.3(3)
C(66)-C(65)-H(65)	119.8
C(64)-C(65)-H(65)	119.8
C(65)-C(66)-C(61)	119.8(3)
C(65)-C(66)-H(66)	120.1
C(61)-C(66)-H(66)	120.1
C(76)-C(71)-C(72)	120.0(2)
C(76)-C(71)-P(6)	120.61(18)
C(72)-C(71)-P(6)	119.03(18)
C(73)-C(72)-C(71)	119.9(2)
C(73)-C(72)-H(72)	120.1
C(71)-C(72)-H(72)	120.1
C(72)-C(73)-C(74)	120.0(2)
C(72)-C(73)-H(73)	120.0
C(74)-C(73)-H(73)	120.0
C(75)-C(74)-C(73)	120.3(2)
C(75)-C(74)-H(74)	119.9
C(73)-C(74)-H(74)	119.9
C(74)-C(75)-C(76)	120.6(2)
C(74)-C(75)-H(75)	119.7
C(76)-C(75)-H(75)	119.7
C(75)-C(76)-C(71)	119.3(2)
C(75)-C(76)-H(76)	120.3
C(71)-C(76)-H(76)	120.3

Symmetry transformations used to generate equivalent atoms:

#1 -x+2,-y+1,-z+1

Table 4: Anisotropic displacement parameters ($Å^2$x 10^3) for S13045. The anisotropic displacement factor exponent takes the form: $-2p^2[h^2 a^{*2}U^{11} + ... + 2 h k a^* b^* U^{12}]$

	U^{11}	U^{22}	U^{33}	U^{23}	U^{13}	U^{12}
Pt(1)	11(1)	10(1)	10(1)	0(1)	3(1)	0(1)
P(1)	14(1)	11(1)	12(1)	-1(1)	3(1)	-2(1)
O(1)	22(1)	22(1)	17(1)	-10(1)	6(1)	-6(1)
B(1)	20(1)	21(1)	16(1)	-6(1)	5(1)	-3(1)
F(1)	34(1)	35(1)	16(1)	-9(1)	2(1)	-10(1)
F(2)	25(1)	42(1)	44(1)	-3(1)	12(1)	11(1)
O(2)	41(1)	24(1)	11(1)	-3(1)	4(1)	-13(1)
P(2)	13(1)	15(1)	9(1)	-1(1)	3(1)	-1(1)
O(3)	15(1)	30(1)	14(1)	6(1)	3(1)	-3(1)
B(2)	14(1)	22(1)	14(1)	1(1)	5(1)	1(1)
F(3)	26(1)	25(1)	26(1)	0(1)	3(1)	10(1)
F(4)	19(1)	39(1)	19(1)	3(1)	8(1)	-9(1)
O(4)	14(1)	20(1)	14(1)	1(1)	3(1)	-5(1)
O(5)	14(1)	17(1)	26(1)	-10(1)	3(1)	-1(1)
P(3)	11(1)	13(1)	10(1)	0(1)	3(1)	-1(1)
O(6)	13(1)	20(1)	16(1)	4(1)	1(1)	-2(1)
B(3)	20(1)	26(1)	14(1)	6(1)	-2(1)	-8(1)
F(5)	18(1)	64(2)	58(1)	41(1)	-4(1)	-5(1)
F(6)	94(2)	44(1)	27(1)	-18(1)	27(1)	-39(1)
O(7)	15(1)	21(1)	18(1)	6(1)	-1(1)	-3(1)
O(8)	26(1)	28(1)	14(1)	6(1)	8(1)	12(1)
P(4)	12(1)	13(1)	12(1)	2(1)	2(1)	-1(1)
O(9)	25(1)	17(1)	19(1)	5(1)	-1(1)	-6(1)
B(4)	25(1)	17(1)	20(1)	2(1)	4(1)	-6(1)
F(7)	55(1)	20(1)	39(1)	10(1)	-9(1)	-13(1)
F(8)	24(1)	67(2)	31(1)	-5(1)	10(1)	-3(1)
O(10)	29(1)	13(1)	20(1)	0(1)	0(1)	-5(1)
P(5)	15(1)	15(1)	15(1)	2(1)	2(1)	0(1)
C(1)	18(1)	18(1)	18(1)	2(1)	4(1)	2(1)
C(2)	31(1)	19(1)	27(1)	2(1)	14(1)	3(1)

C(3)	40(2)	24(1)	34(2)	2(1)	23(1)	6(1)
C(4)	27(1)	28(1)	27(1)	7(1)	13(1)	3(1)
C(5)	21(1)	23(1)	24(1)	4(1)	5(1)	-2(1)
C(6)	21(1)	20(1)	23(1)	0(1)	6(1)	-1(1)
C(11)	17(1)	16(1)	16(1)	1(1)	2(1)	1(1)
C(12)	20(1)	17(1)	16(1)	3(1)	2(1)	0(1)
C(13)	25(1)	18(1)	18(1)	2(1)	-2(1)	1(1)
C(14)	22(1)	23(1)	21(1)	-3(1)	-2(1)	5(1)
C(15)	16(1)	26(1)	21(1)	-2(1)	1(1)	2(1)
C(16)	18(1)	21(1)	18(1)	2(1)	3(1)	0(1)
C(21)	18(1)	17(1)	16(1)	1(1)	2(1)	1(1)
C(22)	19(1)	22(1)	19(1)	0(1)	4(1)	1(1)
C(23)	25(1)	24(1)	21(1)	-3(1)	6(1)	-1(1)
C(24)	29(1)	26(1)	21(1)	-3(1)	2(1)	-1(1)
C(25)	23(1)	30(1)	22(1)	-2(1)	-4(1)	0(1)
C(26)	19(1)	23(1)	21(1)	-2(1)	0(1)	4(1)
C(31)	17(1)	15(1)	20(1)	2(1)	3(1)	1(1)
C(32)	17(1)	21(1)	24(1)	6(1)	3(1)	3(1)
C(33)	24(1)	22(1)	34(1)	9(1)	8(1)	5(1)
C(34)	30(1)	18(1)	41(2)	2(1)	13(1)	1(1)
C(35)	31(1)	20(1)	34(1)	-3(1)	4(1)	-4(1)
C(36)	26(1)	19(1)	25(1)	1(1)	-1(1)	-1(1)
P(6)	18(1)	16(1)	12(1)	-1(1)	2(1)	1(1)
C(41)	20(1)	21(1)	16(1)	-2(1)	4(1)	1(1)
C(42)	28(1)	22(1)	20(1)	-1(1)	7(1)	-4(1)
C(43)	34(1)	27(1)	26(1)	0(1)	10(1)	-9(1)
C(44)	25(1)	42(2)	33(1)	-1(1)	11(1)	-8(1)
C(45)	25(1)	39(2)	39(2)	-3(1)	16(1)	3(1)
C(46)	24(1)	26(1)	31(1)	1(1)	10(1)	4(1)
C(51)	19(1)	16(1)	15(1)	-1(1)	0(1)	0(1)
C(52)	26(1)	22(1)	15(1)	1(1)	0(1)	0(1)
C(53)	31(1)	29(1)	21(1)	4(1)	-7(1)	-3(1)
C(54)	22(1)	27(1)	34(1)	12(1)	-6(1)	-4(1)
C(55)	19(1)	24(1)	34(1)	6(1)	4(1)	1(1)
C(56)	19(1)	22(1)	22(1)	1(1)	4(1)	2(1)
C(61)	22(1)	19(1)	16(1)	1(1)	5(1)	1(1)

C(62)	25(1)	17(1)	22(1)	1(1)	5(1)	-1(1)
C(63)	33(1)	18(1)	34(1)	-4(1)	13(1)	-4(1)
C(64)	41(2)	16(1)	37(2)	2(1)	23(1)	5(1)
C(65)	41(2)	22(1)	32(1)	6(1)	13(1)	12(1)
C(66)	31(1)	26(1)	21(1)	1(1)	3(1)	9(1)
C(71)	18(1)	20(1)	13(1)	-1(1)	1(1)	-1(1)
C(72)	28(1)	23(1)	16(1)	-1(1)	4(1)	-8(1)
C(73)	31(1)	28(1)	16(1)	-2(1)	6(1)	-7(1)
C(74)	30(1)	26(1)	13(1)	-3(1)	2(1)	-2(1)
C(75)	28(1)	20(1)	16(1)	-3(1)	0(1)	-3(1)
C(76)	22(1)	20(1)	16(1)	-2(1)	1(1)	-2(1)

Table 5: Hydrogen coordinates (x 10^4) and isotropic displacement parameters (Å^{2}x 10 ^{3}) for S13045.

	x	y	z	U(eq)
H(2)	8513	9063	2011	29
H(3)	7357	8735	2600	37
H(4)	6896	7458	2622	32
H(5)	7536	6497	2007	27
H(6)	8642	6820	1356	25
H(12)	10005	7134	2360	21
H(13)	11289	6600	2933	25
H(14)	12572	6934	2549	27
H(15)	12594	7826	1602	25
H(16)	11317	8350	1014	23
H(22)	10498	7363	158	24
H(23)	10121	6832	-1001	27
H(24)	8714	6917	-1587	30
H(25)	7680	7532	-1022	31
H(26)	8042	8062	140	25

H(32)	8855	9388	170	25
H(33)	8963	10743	181	32
H(34)	9867	11372	1099	34
H(35)	10681	10654	2016	34
H(36)	10550	9304	2039	29
H(42)	8259	11246	4453	28
H(43)	9325	11669	3800	34
H(44)	10205	10763	3345	39
H(45)	10066	9443	3573	40
H(46)	9027	9012	4255	31
H(52)	7064	9941	3373	25
H(53)	5744	10246	2707	34
H(54)	4618	10631	3299	34
H(55)	4827	10784	4556	31
H(56)	6144	10467	5239	25
H(62)	6629	8626	3999	25
H(63)	6589	7265	3978	33
H(64)	7556	6558	4789	35
H(65)	8581	7191	5605	37
H(66)	8641	8540	5630	31
H(72)	7050	9148	6100	27
H(73)	7018	9587	7283	30
H(74)	7682	10753	7673	27
H(75)	8412	11465	6899	26
H(76)	8453	11038	5712	23

REFERENCES

(1) Harvey, E. L. Dissertation (Ph.D.), California Institute of Technology, 1990.

(2) Durrell, A. C.; Keller, G. E.; Lam, Y.-C.; Sykora, J.; Vlček, A.; Gray, H. B. *J. Am. Chem. Soc.* **2012**, *134*, 14201.

(3) Lam, Y.-C., Caltech, 2015.

(4) Lam, Y.-C.; Darnton, T. Unpublished results.

(5) Pinto, M. A. F. D. R.; Sadler, P. J.; Neidle, S.; Sanderson, M. R.; Subbiah, A.; Kuroda, R. *J. Chem. Soc. Chem. Comm.* **1980**, 13.

(6) Lakowicz, J. R. *Principles of Fluorescence Spectroscopy*; Springer US, 2006.

(7) Dawson, W. R.; Windsor, M. W. *J. Phys. Chem.* **1968**, *72*, 3251.

(8) Ware, W. R.; Baldwin, B. A. *The Journal of Chemical Physics* **1965**, *43*, 1194.

(9) Crosby, G. A.; Demas, J. N. *J. Phys. Chem.* **1971**, *75*, 991.

(10) Brouwer, A. M. *Pure and Applied Chemistry* **2011**, *83*.

(11) Murov, S. L., University of Chicago, 1967.

(12) Lampert, R. A.; Chewter, L. A.; Phillips, D.; O'Connor, D. V.; Roberts, A. J.; Meech, S. R. *Analytical Chemistry* **1983**, *55*, 68.

(13) Eaton, D. F. *Pure and Applied Chemistry* **1988**, *60*, 1107.

(14) Greiner, G. *Journal of Photochemistry and Photobiology A: Chemistry* **2000**, *137*, 1.

(15) Milder, S. J.; Brunschwig, B. S. *J. Phys. Chem.* **1992**, *96*, 2189.

(16) Armarego, W. L. F.; Chai, C. L. L. In *Purification of Laboratory Chemicals (Sixth Edition)*; Butterworth-Heinemann: Oxford, 2009, p 88.

(17) Che, C. M.; Butler, L. G.; Gray, H. B. *J. Am. Chem. Soc.* **1981**, *103*, 7796.

(18) Pangborn, A. B.; Giardello, M. A.; Grubbs, R. H.; Rosen, R. K.; Timmers, F. J. *Organometallics* **1996**, *15*, 1518.

(19) Che, C. M.; Schaefer, W. P.; Gray, H. B.; Dickson, M. K.; Stein, P. B.; Roundhill, D. M. *J. Am. Chem. Soc.* **1982**, *104*, 4253.

(20) Sheldrick, G. *Acta Crystallographica Section A* **1990**, *46*, 467.

(21) Sheldrick, G. M. *Acta Crystallogr A* **2008**, *64*, 112.

(22) Müller, P. *Crystallography Reviews* **2009**, *15*, 57.

(23) Cobas, J. C.; Sardina, F. J. *Concepts in Magnetic Resonance Part A* **2003**, *19A*, 80.